geosciences

MDPI

Article

Analysis of the Influence of Structural Geology on the Massive Seismic Slope Failure Potential Supported by Numerical Modelling

Emilie Lemaire [1,*], Anne-Sophie Mreyen [1], Anja Dufresne [2] and Hans-Balder Havenith [1]

[1] Department of Geology, University of Liege, 4000 Liege, Belgium; as.mreyen@uliege.be (A.-S.M.); hb.havenith@uliege.be (H.-B.H.)
[2] Department of Engineering Geology and Hydrogeology, RWTH Aachen University, 52062 Aachen, Germany; dufresne@lih.rwth-aachen.de
* Correspondence: emilie.lemaire@student.uliege.be

Received: 18 June 2020; Accepted: 13 August 2020; Published: 18 August 2020

Abstract: The stability of rock slopes is often guided significantly by the structural geology of the rocks composing the slope. In this work, we analysed the influences of structural characteristics, and of their seismic responses, on large and deep-seated rock slope failure development. The study was focused on the Tamins and Fernpass rockslides in the European Alps and on the Balta and Eagle's Lake rockslides in the southeastern Carpathians. These case studies were compared with catastrophic rock slope failures with ascertained or very likely seismic origin in the Tien Shan Mountains. The main goals was to identify indicators for seismically-induced rock slope failures based on the source zone rock structures and failure scar geometry. We present examples of failures in anti-dip slopes and along-strike rock structures that were potentially (or partially) caused by seismic triggering, and we also considered a series of mixed structural types, which are more difficult to interpret conclusively. Our morpho-structural study was supported by distinct element numerical modelling that showed that seismic shaking typically induces deep-seated deformation in initially "stable" rock slopes. In addition, for failures partially triggered by dynamic shaking, these studies can help identify the contribution of the seismic factor to slope instability. The identification of the partial seismic origin on the basis of the dynamic response of rock structures can be particularly interesting for case histories in less seismically active mountain regions (in comparison with the Andes, Tien Shan, Pamirs), such as in the European Alps and the Carpathian Mountains.

Keywords: deep-seated failure; bedding and joint orientation; seismic deformation; structural analysis; discrete element modelling

1. Introduction

Rockslides occur in many mountain regions of the world [1–6] and are defined as large, mostly translational bedrock landslides including large volumes of debris (up to billions m^3) [7–9]. The exact cause of slope failure (if prehistorical) is often unclear. They can be triggered by several and diverse factors, and most of the time there is not a single cause but rather a combination of geological, morphological, physical, and/or human factors that prepare a slope for failure. We distinguish trigger (near-immediate causes of a slope failure) and preparatory or preconditioning factors (background conditions and long-term actions). Whereas the definition of landslide sizes is discussed in various works in relation to their debris volume or slope height, e.g., Davies and McSaveney [10] and Korup et al. [11], herein we use the term massive for large volumes > 10^7 m^3. The presented massive rock slope failures are influenced by factors that condition slope instability depending on the

structural geology and the history of weathering, erosion, climate, seismo-tectonic damage, glacial debuttressing, and human activities, combined with triggering factors linked to an external stimulus, such as earthquakes, intense rainfall, dam construction, or a similar short-term action. One of the most important preconditioning factors influencing the stability of rock slopes is the orientation of discontinuities (bedding planes, joints, or faults) within the geological material. In this paper, we review the structural features of the source zones of selected case studies that could indicate a seismic trigger for these large rock slope failures. Therefore, deep-seated and massive failures especially are analysed with regard to their structural characteristics. We analyse in detail a possible seismic origin for the Tamins and Fernpass giant rockslides, located, respectively, in the Swiss and Austrian Alps, and an origin for the Balta and Eagle's Lake rockslides in the SE Carpathian (see location in Figure 1). For comparisons, we review case studies from the presented regions wherein rockslides were demonstrably triggered by earthquakes (e.g., Rawhilhorn and Dobratsch located, respectively, in the Swiss and Austrian Alps). In addition, examples of the Tien Shan are discussed, as this region is one of the prime reference areas for co-seismic rockslides. The main goals of this work were to analyse the influences of rock structures on the stability of a slope during seismic events and to identify structural and geological characteristics of the source zone that could, with more dedicated work on these features, help prove a partial or pure seismic origin for prehistoric rockslides with a reasonable level of confidence.

Figure 1. Geographical locations in Europe of the Tamins, Tour d'Aï, and Rawilhorn rockslides (Switzerland); the Fernpass and Dobratsch rockslides (Austria); and the Eagle's Lake and Balta rockslides (Romania).

Earthquake-induced rockslides can be found in all mountainous regions affected by at least medium (maximum peak ground acceleration $\geq$ 0.1 g , or maximum intensity $\geq$ VII for a 475 year period) seismic hazard conditions (see some cases in Table A1, in the Appendix A), and often represent some of the most disastrous geohazards in these regions [5,12]. The Daguanbao rockslide (China) was the largest co-seismic landslide triggered by the 2008 Wenchuan earthquake [13]. Cui et al. [13] studied the geological factors of the Daguanbao rockslide. Their results reveal that the source rock structures, including three joint sets, local faults, and folds in the landslide zone, had a potential influence on the failure mechanism of the slide. The combination of joint sets allowed for a large wedge failure with sliding along lateral boundaries (joints with striking sub-parallel to the sliding direction). However, none of the discontinuities were really favourable for a failure under static conditions (no discontinuity with 25–50° dip oriented parallel to the sliding direction). In a seismically-triggered rockslide, the geological structure is commonly considered to be one of the factors that determines the initiation and kinematics of the slide [12,14,15]. An example where both geological background

conditions and seismic triggering resulted in a catastrophic rockslide event is the Dobratsch landslide in the Austrian Alps in 1348 [16].

2. Geological Context of Studied Rockslides

2.1. Rockslides in the European Alps: Historical Examples of Earthquake-Triggered Mass Movements

Earthquakes in the European Alps commonly occur at depths of 20 km [17] and have reached magnitudes of >6 in historic times (e.g., Friuli 1976 and Sierre 1946); such magnitude earthquakes can trigger landslides up to 50 km away from the epicentre [18]. There is a long record of landslide disasters in historical and recent times in the European Alps, but there are only a few documented cases of larger rockslides triggered by earthquakes. For instance, in 1348, six landslides (with volumes of 1, 3.5, 8, 15, 20, and 100 mio m^3) were triggered in the Dobratsch Mountain [18] (Figure 2) by an earthquake in the Friuli region (northern Italy) [16]. Two other seismically-triggered mass movements in the Swiss Alps were the 1946 Rawilhorn (Figure 2) and 1584 Tour d"Aï rockslides; the latter reportedly killed a few hundred people [19].

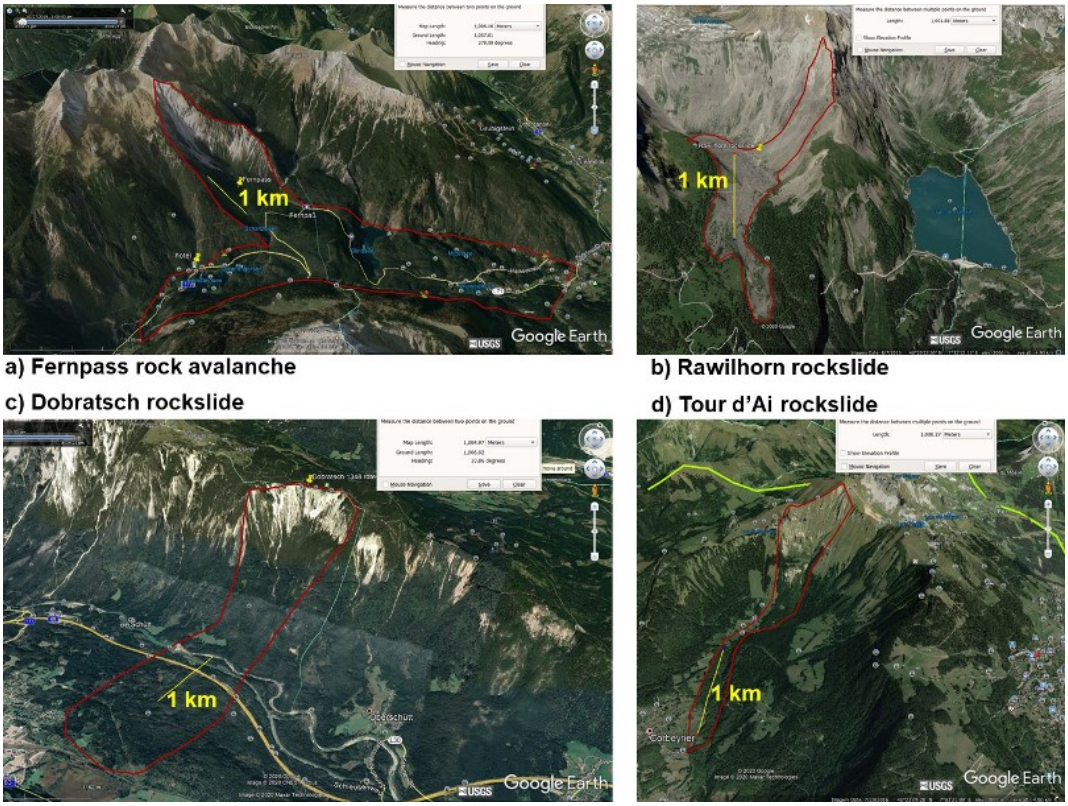

Figure 2. Large (>10^7 m^3) rockslides in the Alps with possible or confirmed seismic origins: (**a**) Fernpass rockslide, Austria, with possible seismic origin due to age and structures (not related to glacier retreat); (**b**) Rawilhorn rockslide triggered by the 1946 Sierre earthquake; (**c**) Dobratsch rockslide triggered near Villach (Austria) by a M∼7 earthquake in the Friuli region in 1348; (**d**) Tour d"Ai rockslide triggered by the 1584 Aigle (Switzerland) earthquake (with uncertain outline).

In Switzerland and its close surrounding countries, the Swiss Seismological Service registers an average number of 500 to 800 earthquakes per year with magnitudes of 2.5 or more [17]. In the Swiss Alps, seismicity is located mainly in the Valais and Grisons regions [17]. Some of these earthquakes have triggered landslides, such as the aforementioned Sierre event in 1946. However, most landslides in the European Alps have a climatic origin. For Switzerland, Badoux et al. [20] showed that 7% of all fatalities due to natural hazards are caused by landslides (of any origin), and Lateltin et al. [21] estimated that more than 6% (2500 km^2) of Switzerland has been affected by landslides. In Switzerland,

an earthquake with a magnitude of 6 or more generally occurs every 50 to 150 years and magnitude seven earthquakes are expected to be 10 times less frequent, and actually, have never been observed in historical times [17].

In the eastern Swiss Alps (Grisons region), the ancient Tamins rockslide (see location in Figure 1; more detailed views are shown in the third section) with a volume exceeding around 1.5 km^3 [2] had an unknown trigger but presents some characteristics (deep scarp compared to other rockslides in the Alps, high on the slope, and not clearly undercut by a river) of a mass movement with at least partial seismic influence. This rockslide collapsed from the Sennenstein Mountain and blocked the Rhine Valley. Even though the Tamins rockslide was a very large mass movement, it is far less studied than its "big brother", the Flims slide that occurred in same area but with an estimated volume of 8–12 km^3 [22–24]. It is assumed that the Tamins event influenced the Films rockslide through the formation of a dam on the Rhine River and the related impounding of a lake [25]. Poschinger and Haas [26], Deplazes et al. [27], and Ivy-Ochs et al. [28] have dated the Flims event between 8000 and 10,100 cal yrs BP (see Table 1), and Poschinger et al. [22] stated that Tamins is about the same age as Flims, but most likely slightly older. On the map (Figure A1a, in the Appendix B) by Hetényi et al. [29] the Tamins rockslide is located near thrust fault systems, but not specifically near active faults (the source zones are not crossed either by active or by ancient faults). The fault appears to run upstream from the rockslide. Krietsch and Wolter [25], in their article, also mention a NS-striking dextral fault zone located at the Kunkelspass and a WSW-ENE striking fold axis.

Table 1. Age ranges determined for the Flims rockslide.

Age [cal ka BP]	Method	Reference
8210–10,100 cal yrs BP	^{14}C of tree trunks below landslide boulders at the deposit edge	Poschinger and Haas [26] Deplazes et al. [27]
8400–9050 cal yrs BP	^{14}C of supra-landslide lake deposit	Deplazes et al. [27]
8200–9520 cal yrs BP	^{36}Cl and ^{10}Be exposure dating of landslide scarp and deposit boulders	Ivy-Ochs et al. [28]

In the western Austrian Alps, the 1 km^3 Fernpass rockslide (Figure 1) is also marked by a deep-seated scarp cutting into thick layers of dolomites, limestones, and marls [30]. The event occurred 4100–4200 years ago [16]. The rock mass of this slope failure, after oblique collision with the opposite valley flank, split into two separate arms that travelled 12 km towards the north and 15.5 km towards the south, respectively. At the place of collision, the avalanche deposits are still lying about 100–200 m higher than along the two neighbouring tongues but the initial run up is likely to have been much higher; this zone is now covered by vegetation (observed from Google Earth®). The Fernpass rockslide is part of a spatial cluster with its adjacent mass movements, including the Eibsee, Tschirgant, Tumpen, and Köfels rockslides [16]. Prager [31] mentioned that the particular wedge-shaped scarp suggests the failure not only to depended on the existing bedding conditions, but also on convoluted intersections of fracture and uncemented fault systems. Prager et al. [16] also mentioned the possibility of a local earthquake in the area, close to the Fernpass, but the exact trigger is still debated with the climate cause. Prager et al. [16] stated that field investigations do not suggest any signs of a smoothed morphology for both the rough scarp and the intensely structured accumulation area, and thus do not indicate glacial overprinting. This evidence of no glacial overprinting is also relevant for many landslides in the cluster, and thus means they were not directly induced by Late-Pleistocene glacier fluctuations [16]. The area of the Austrian Western Alps consists of complex fold and thrust belts of different nappe units with main geological structures formed by Cretaceous to Tertiary thrust and extension tectonics (Figure A1b) [16]. On the map (Figure A1a, in the Appendix B) by Hetényi et al. [29] the Fernpass rockslide is located near thrust fault systems. Both maps from [29] and [16] (Figure A1, in the Appendix B) show that several faults are present downstream from the Fernpass rockslide.

2.2. Rockslides in the Se Carpathians: Historical Examples of Earthquake-Triggered Mass Movements

The SE bend of the Carpathian Mountains belt ("Curvature Carpathians"), Romania, shows possibly the highest sub-crustal earthquake activity in Central Europe [32]. Even though the region presents a comparatively smooth relief, it is prone to slope instabilities conditioned by intense precipitation and floods, but also by seismic events [33,34]. The herein studied Vrancea-Buzau region especially is known to be seismogenic, and numerous intermediate-depth events were registered in the last three centuries. Magnitudes of these events varied between Mw 7.4–7.9 with intensities of I = IX − X MSK [35–37]. Historic reports of the 18th century and the 1802 and 1838 Vrancea earthquakes only list various damages and casualties in densely populated areas, whereas for the 1940 (7.8 Mw, hypocentral depth 90 km) and 1977 (7.5 Mw, hypocentral depth 95 km), geohazards such as groundwater fluctuations, floods, liquefaction, and landslides are also documented [35,36,38–41]. According to Mândrescu [38], several reactivated or new landslides (e.g., *Slon*, *Zăbala*-both forming landslide dams in the valley) and rock falls (e.g., *Siriu*, *Calvini*) have been induced by the 1977 quake. The landslides are described as rather superficial failures with relatively small surface areas.

Herein, we concentrate on the case studies of Balta and Eagle's Lake rockslides, both deep-seated failures located in the Flysch Carpathians. Although of unknown historical origin, they are marked by geomorphic and structural features that could imply co-seismic failure. The geological setting of the region is marked by multiple reverse faults striking SW–NE, and left lateral strike-slip faults orientated nearly perpendicular to the latter in a NW–SE direction, as illustrated in Figure 3.

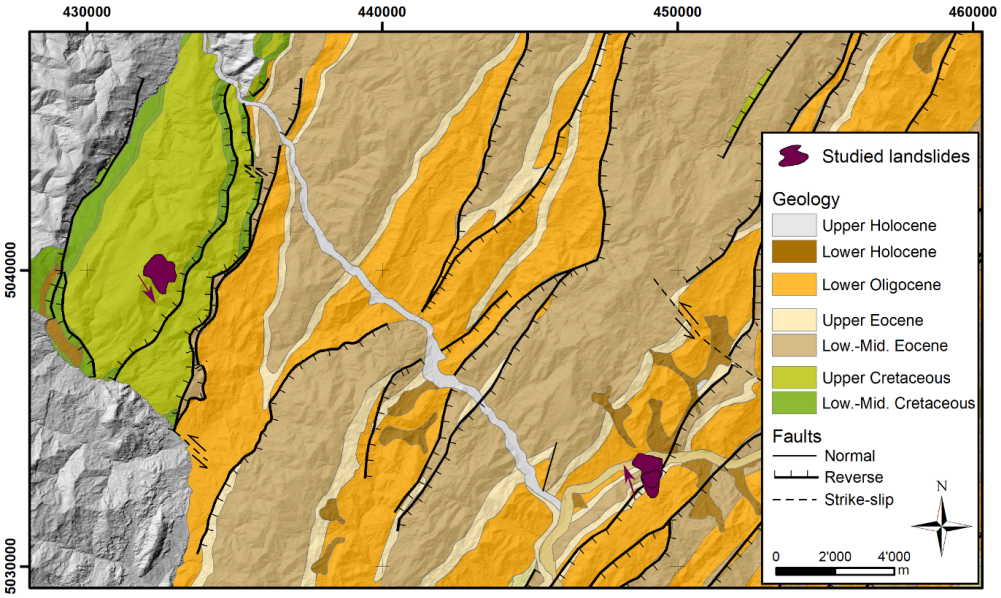

Figure 3. Geological map of the study area in the SE Carpathians (Buzau province; modified after [42]) with the Eagle's Lake in the west and the Balta rockslide in the east of the map (coordinate system: UTM 35N). The arrows mark the sense of landslide motion.

The Balta rockslide is located in the vicinity of past epicentres (e.g., about 35 km and 50 km SW of the 1940 and 1977 events, respectively). It developed in a Paleogene schistose sandstone flysch marked by thick sandstone banks (Figure 3); one reverse fault crosses the upper part of the Balta rockslide source zone, dipping into the slope. A pronounced head scarp developed close to the mountain ridge and shows a 40°–50° inclined anti-dip bedding orientation. A major part of the fragmented rockslide mass accumulated in the middle part of the slope (forming a *plateau*), while the rockslide front spreads into the valley and might have formed a dam blocking the river in the past [43]. The typical hummocky morphology of the rockslide deposit distinguishes itself from the vast number of superficial flows and slides typical for the region.

The Eagle's Lake rockslide (*Lacul Vulturilor*; located 18 km WNW from Balta, Figure 3) developed in Upper Cretaceous sandstone flysch along a SW–NE striking synclinal axis constituting the summit of the massif. East from the site, two reverse faults thrust the Cretaceous flysch layers over Upper Paleogene layers. The Eagle's Lake rockslide presents a pronounced scarp area that also developed in an anti-dip slope (20° dip of bedding to the NW with a rockslide that failed to the SE). Below this scarp, the rockslide body (forming a small plateau in the upper part) is marked by hummocky morphology and hosts one silted-up and one existing supra-landslide lake. Near this site, some recent rockfalls have been observed and graben structures can be found directly behind the crest above the scarp. In the 20th century, various theories of the site's genesis were discussed, such as a glacial or erosional origin (e.g., [44]). Sîrcu [45] suggested its present geomorphology to be a combined result of ancient and recent landslide activities.

2.3. Typical Large Rockslides Triggered by Earthquakes in the Tien Shan

As indicated above, there are only a few historical cases of large (with a volume of at least 10^6 m^3) rockslides with proven earthquake triggers in the European Alps and no cases for the SE Carpathians. Therefore, some characteristic features will be outlined on the basis of previous studies [46,47] for rockslides in the Tien Shan Mountains, Central Asia. However, even for these regions where large rockslides triggered by earthquakes are more common than those induced by, e.g., climatic events, we cannot conclusively ascertain a seismic origin for all giant mass movements.

As indicated by Havenith et al. [46], the first records of seismically induced landslides exist for the M = 6.9 Belovodsk earthquake (located in Figure 4) that hit the northern slopes of the Tien Shan in 1885 [48]. According to contemporaneous reports and oral accounts, the earthquake caused many slope failures, but it is not known whether it also triggered the two neighbouring Bielogorka rock avalanches (see Google Earth® view shown in Figure 5a) located close to the village at a distance of less than 15 km. Even tree ring dating (dendrochronological analysis—unpublished data) on the tongues completed in summer 1998 did not yield results that allow one to elucidate this uncertainty. Strom and Abdrakhmatov ([5]; see p. 162) tried to date those rock avalanches again via dendrochronology in 2009, but the results were the same as in 1998—all dated trees were not older than 70. Outcrops close to the mass movements and samples from the tongue show that the failed rocks are principally made of sandstone, locally crossed by andesitic dykes. We are almost sure that these "twin" rock avalanches occurred at the same time as the tips of their tongues moved side by side; they do not overlap and obviously pushed each other away—and this contemporaneity clearly hints at a seismic origin. The detachment scarps of these failures are more than 600 m high and wide for rock avalanche 1 (RA1), and 400 m high and wide for rock avalanche 2 (RA2). The summit of the RA1 scarp is located at a rock promontory, whereas the top of the RA2 scarp almost exactly follows a mountain crest. The entire volume of RA1 is about 30×10^6 m^3, and RA2 amounts to about 15×10^6 m^3. Structural data for discontinuities collected in the area and within the scarp of RA2 reveal two main orientations of joints [46]. Here, we highlight only the fact that all discontinuities principally dip into the slope and do not delineate a potential failure volume. Furthermore, the sandstones presented little evidence of weathering; only some andesitic dykes were affected by weathering. The two rock avalanches are not only spectacular slope failures due to their large volume but also due to the geometry of the displaced material. A remarkable feature of RA1 is a block of several million m^3 remaining inside the landslide scarp.

The second case history is related to the Kemin Ms = 7.8–8.2 earthquake in 1911 (Figure 4). This earthquake caused numerous landslides and rockfalls along the Chon Kemin strike-slip fault and the Chon Aksu reverse fault (dipping to the north), activated in total over a length of more than 200 km. The largest mass movements triggered by this event were those of Ananevo and Kaindy. One more rockslide of a similar size was triggered by the same earthquake along the Chilik River valley in Kazakhstan. The first rock avalanche (about 15×10^6 m^3) made of limestone occurred on the slope above the activated Chon Kemin fault (E–W rupture zone shown in Figure 4) about 60 km

west of the epicentre, and buried a village of yurts with 38 inhabitants. The second, non-fatal rockslide was the one of Ananevo shown in Figure 5b that developed in granitic rocks. Rock structures of the latter, and the measured and simulated seismic response of the whole mountain site that produced this rockslide, are described in detail in Havenith et al. [49]. As for the Bielogorka rock avalanches, here we indicate only that none of the discontinuities observed within the scarp area are favourably oriented for sliding. Havenith et al. [50] show that the site must have been highly stable under static conditions and that a major slope failure could only develop at depth by creation of a sliding surface crossing existing structures by breaking rock blocks, notably thanks to a deeper weathering of the granitic rocks that would have facilitated these breaking processes.

The rockslide shown in Figure 5c was triggered by the most recent M > 7 (Ms = 7.1–7.3) earthquake in the Tien Shan, on 19 August 1992, about 100 km southwest of Bishkek (Figure 4). This rockslide affected the headwater slopes of the Belaldy River and later led to formation of a disastrous debris flow killing about 35 people, more than a half of all casualties caused by the event [51]. The Belaldy rockslide formed in massive granitic rocks; thus, the sliding surface did not develop on any particular lithological limit. During a site visit in 2009, we found that some joint sets are oriented parallel to the sliding plane and could thus have structurally predisposed this failure.

The almost 2000 km long Talas-Fergana Fault (TFF) crossing the Tien Shan in the NW–SE direction has not produced any historical earthquake, but a series of paleoseismic deformations, such as up-slope facing scarps and fault scarps and horizontal displacements of the relief forms, together with numerous seismogravitation forms such as rockslides and landslides, have been outlined by Korjenkov et al. [52]. Korzhenkov et al. [53] also considered the Karasuu rock avalanche (Figure 5d) to be the result of an earthquake that would have occurred, according to their dating, about 1500 years ago (using also as input data the lichonometric analysis of Belousov et al. [54]). They described the source area of the Karasuu rock avalanche as an "amphitheatre-like scar" that is located on the left slope (dipping to the northeast) of the Karasuu River valley. "Amphitheatre-like" also describes quite well the form of the source zone of the Bielogorka rock avalanche RA1 (imagining it without the block in the middle), of the Fernpass rock avalanche and the Tamins rockslide in Alps, and of the Balta rockslide in Romania. According to Korzhenkov et al. [53], this "amphitheatre-like" deep cut (marking a very deep-seated wedge-like but also rounded scarp) in the rock layers is often considered as a marker of the seismic origin of a rockslide, as it could be an indication of external forces to create this scarp geometry that is not defined by structural elements—the validity of this assumption will be discussed further below. Korzhenkov et al. [53] indicated that the Karasuu dam was formed by a rock avalanche on the Karasuu River, and it blocks the large lake with the same name which stretches over almost 7 km along the TFF. The dam is about 2000 m long, 1000 m wide, and 200 m thick; it would have a total volume of 200 to 400 million m^3 (the first estimate according to Strom and Abdrakhmatov [5], the second according to Korzhenkov et al. [53]; it should be noted that Havenith et al. [55] calculated a smaller volume of only 130 million m^3). While considering the origin of the Karasuu rock avalanche as being related to an earthquake, Korzhenkov et al. [53] also noted that "[...] ages of rockslides are much younger than those of (Middle Holocene) earthquakes [...] that paleo-earthquakes and significant gravity rockslides are not always coeval. Apparently, not all rockslides and rock failures in this region occurred due to historically strong earthquakes, although the latter probably prepared slopes for the subsequent rock failures." This preparatory effect of earthquakes on slope stability was considered in the final conclusions of Korzhenkov et al. [53], as it is one of the main problems hampering the use of old landslides for paleoseismic analyses [53].

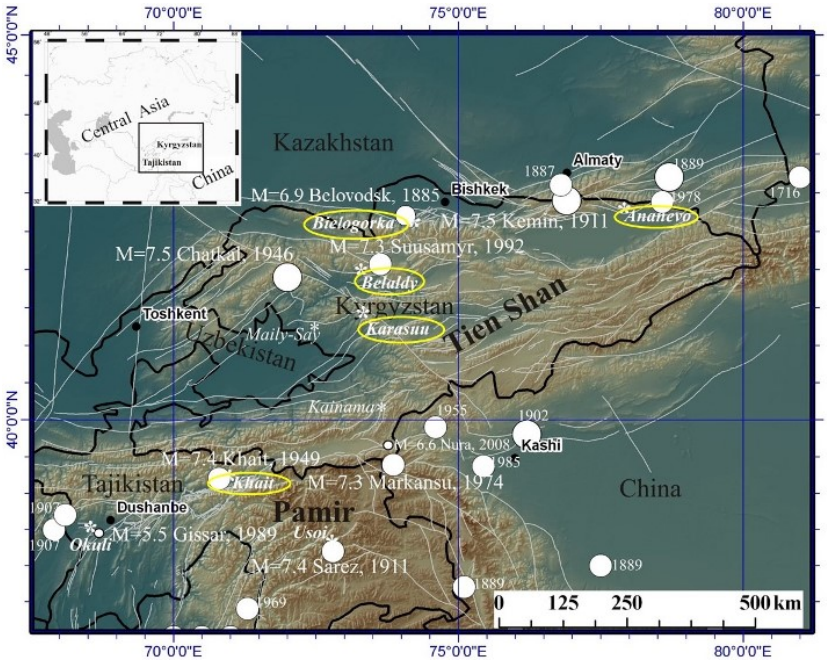

Figure 4. Maps of rockslide locations in the Tien Shan, including examples of proved earthquake-triggered failures: the 1911 Ananevo and 1992 Belaldy rockslides, the 1949 Khait rock avalanche.

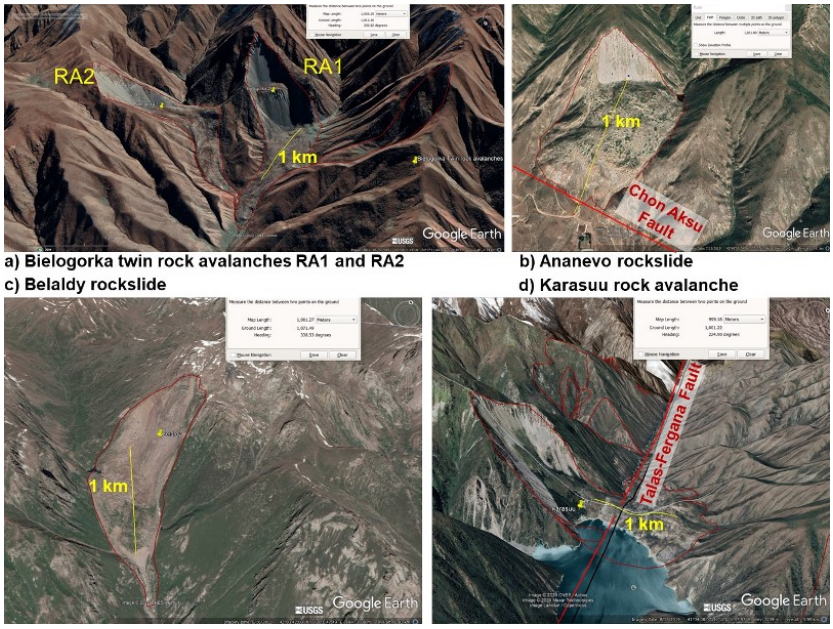

Figure 5. (**a**) Examples of ancient landslides with proven (**b**,**c**) and likely (**a**,**d**) seismic origins: (**a**) the Bielogorka twin rock avalanches RA1 and RA2 (year unknown; if related to the Belovodsk earthquake: 1885); (**b**) the Ananevo rockslide (1911); (**c**) the Belaldy rockslide (1992); (**d**) the Karasuu rock avalanche.

In fact, only two of the four presented proven or likely seismically-triggered rockslides are located near or on an active fault: Ananevo and Karasuu. The Belaldy rockslide occurred quite far from the next surface rupture related to the Suusamyr event, and the Bielogorka twin rock avalanches are located in the first range of higher mountains; the surface rupture occurred in front of the range. However, as the Ananevo rockslide, both the Belaldy and Bielogorka rockslides are located in the hanging wall of the activated thrust fault and strong shaking near-fault effects can be expected for these sites.

3. 3D Views and 3D Geomodels of Studied Rockslides

In order to represent the surface and structural features of the Tamins, Fernpass, Balta, and Eagle's Lake rockslides, we created 3D geomodels of the respective sites with the Leapfrog Geo software (developed by Seequent©). The surface data used for the geomodel constructions were the 11 m-resolution digital elevation model TanDem-X for Balta and Eagle's Lake (from the German Aerospace Center, DLR) and the swissALTI3D for Tamins (from the Federal Office of Topography, swisstopo). The aim of the presented models was to outline the spatial relationships between structural features, such as bedding planes and joint sets, and morphological characteristics of the site. Structural measurements were performed during several field campaigns and results were included in the geomodels by indicating their dip and dip azimuth. The data were displayed on a stereographic projection as disks oriented and inclined according to the strike and dip. A stereographic projection (stereonet) is used to display and handle the 3-dimensional geometry of complex structural data [56]. Here, we work with the Lambert azimuthal equal-area projection that optimises an equal area and helps to evaluate the spatial distribution of structures more easily. This equal area projection is generally referred to as Schmidt Net [57]. With Leapfrog, it is possible to display the Fisher mean and the Bingham best-fit plane on the stereonet. The Fisher statistics represent a symmetrical spherical normal distribution estimating a mean direction [58] usually used for palaeomagnetism. The Bingham best-fit plane is commonly used for the cylindrical best-fit measurement of the fold axes; three eigenvectors are displayed (e1, e2, and e3). The greatest concentration of points is represented by the first axis; the second is for the intermediate concentration; and the third, the smallest concentration; mostly the third axis is interpreted as the cylindrical fold axis [59]. OSXStereonet software was used to produce strike and dip symbols that can be displayed in Google Earth®.

3.1. Geomodel of the Tamins Rockslide

Structural data of the Tamins rockslide were collected in the field and afterwards plotted on Google Earth® images with strike and dip symbols (Figure 6) and on stereonet (Figure 7 and Figure A2, in the Appendix C). These data are composed of bedding, joint, schistosity, and fault measurements.

The results from the stereonet (Figure A2b, in the Appendix C) show that the bedding planes measured on the eastern flank are dipping westwards, whereas near the top of the scarp the bedding is dipping southwards, and on the western flank it is dipping towards the north-west. Figure 7 outlines the different orientations of the bedding planes. Fisher mean planes of each flank were calculated; a N179°E 57°W orientation for the eastern flank, N82°E 45°S orientation for the top of the scarp, and N230°E 50°NW orientation for the western flank. The bedding planes of the eastern flank (Figures 6a and 7a) do not have a favourable trend to a slide and the orientations of the layers in the western flank are also not favourable to sliding (Figures 6c and 7c); however, the bedding planes observed on the top of the scarp (Figures 6b and 7b) show a favourable trend in the direction of sliding. The different orientations of the bedding create bounding surfaces delineating the failure volume. Furthermore, on the top of the western flank some minor bedding failures can be observed, locally combined with rock falls. The recent rockfalls (orange outline in Figure 6) confirm the persistent instability of the upper part of the mountain.

The measurements of the joints plotted on the stereonet present a rather scattered distribution (Figure A2c). The poles' distribution enables us to highlight some trends in the north-east and the west part of the stereonet. This distribution suggests a wedge failure. In addition to that, the Bingham's best-fit plane was applied to outline the plunge of a main intersection of several joint's planes. The analysis produced an axis e3 which has a trend and a plunge value of 143° and 42°, respectively. This e3 axis has a plunge in the same direction as the main sliding orientation of the rockslide. Therefore, the overall average of all discontinuities grouped could be favourable for sliding.

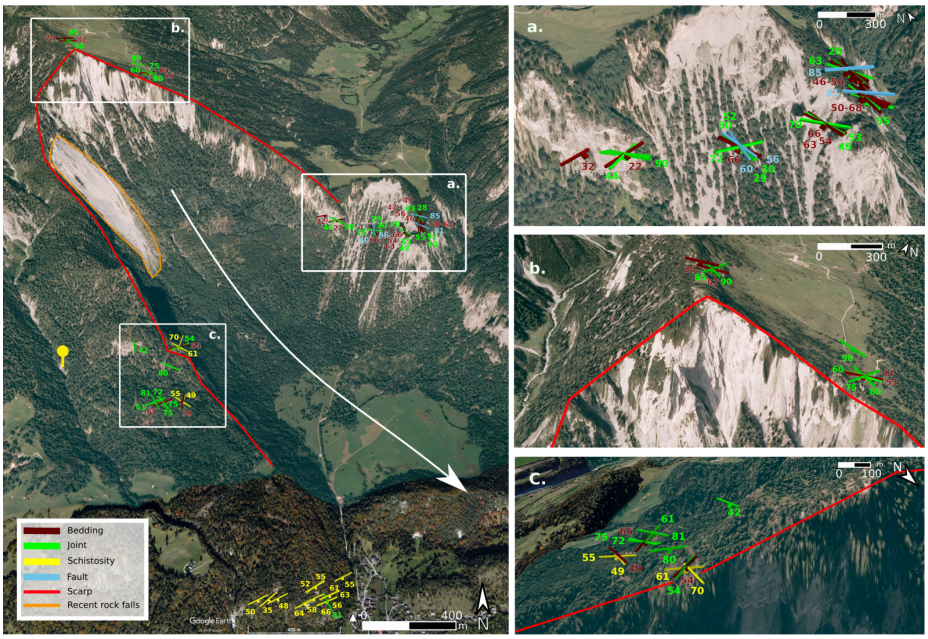

Figure 6. Four Google Earth® views of the Tamins rockslide with the strike-dip symbols of the measurement: global view on the left panel and detailed views of the (**a**) east flank, (**b**) summit, and (**c**) west flank. The numbers near the strike-dip symbols are the values of the dip, and the white arrow displays the direction of the slide. The yellow icon has as coordinates of latitude 46°50′26.56′′ N and longitude 9°23′16.69′′ E.

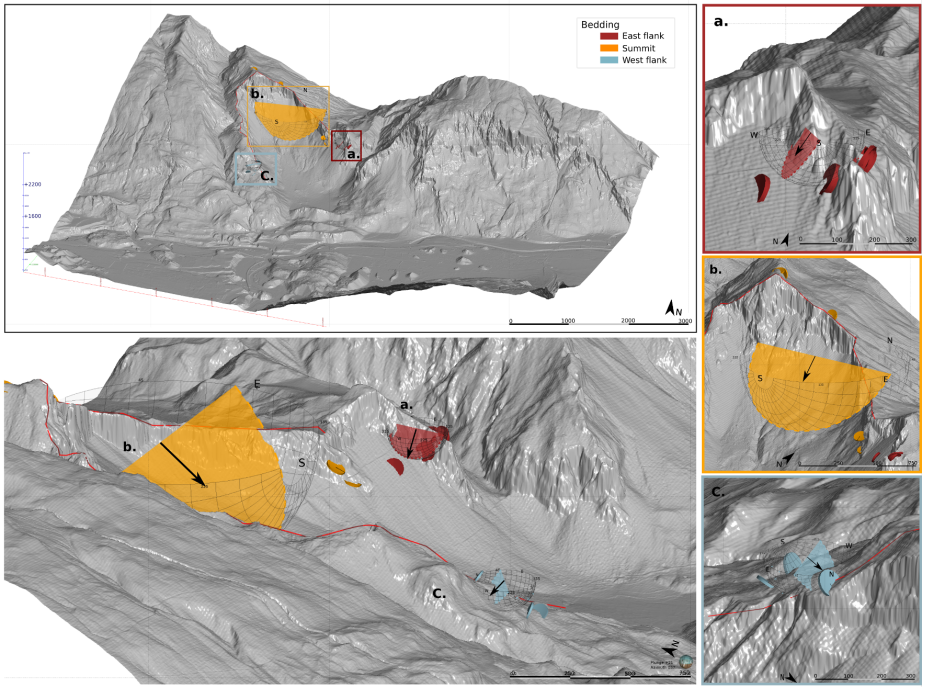

Figure 7. Five different views of the 3D model of the Tamins rockslide: the upper left panel gives a global view of the rockslide and the lower left panel a detailed view of the three stereonets with the bedding of the (**a**) east flank, (**b**) summit, and (**c**) west flank. The colour planes are the Fisher mean planes; the black arrows show the plunge of these planes; and the red line outline the scarp of the rockslide (coordinate system: CH1903+/LV95).

3.2. 3D Views of the Fernpass Rock Avalanche

Structural measurements of the Fernpass rock avalanche show that the bedding is dipping northwards (Fisher mean plane; N275° E 47° N), the joints mainly southwards (Fisher mean plane; N65° E 59° S) and the faults eastwards (Fisher mean plane; N00° E 58° E). The stereonet of the Fernpass rockslide (Figure 8) revealed that the massive rock slope failure occurred along the bedding strike (lateral displacement). Indeed, the sliding has a West-East orientation. Concerning the measured faults, the planes display a favourable trend in the direction of the sliding. There is especially one fault which shows a favourable orientation but has a low dip.

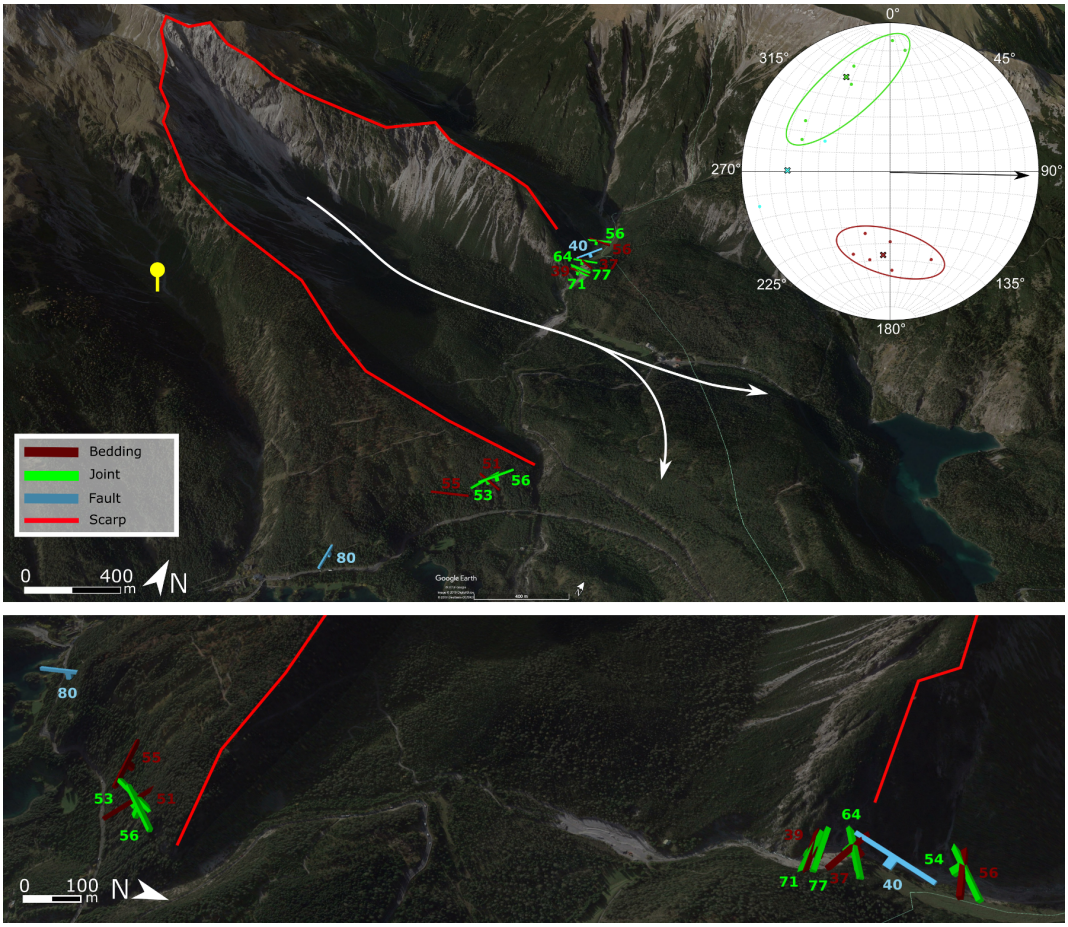

Figure 8. Two Google Earth® views with the strike-dip symbols of the measurement took the Fernpass rock avalanche and a stereonet: the upper image shows a global view the rockslide and the lower image is a zoom on the measurements. The numbers near the strike-dip symbols are the values of the dip and the white arrow displays the direction of the slide. Dots on the stereonet are the poles of the great circles and the black arrow shows the direction of the slide. The yellow icon, on the upper image, has as coordinates of latitude 47°21′8.59″ N and of longitude 10°48′2.63″ E.

3.3. Geomodel of the Eagle'S Lake Rockslide

The Eagle's Lake rockslide presents a large scarp area with a morphology that is most probably overprinted by erosional processes during several hundreds of years (or more), since geomorphological features of the study area are not as pronounced as in comparable but rather fresh failures (<100 years). The slope is an anti-dip slope, wherein bedding structures dip at 10–30° towards NW and a general strike orientation in the NE-SW direction (parallel to the synclinal north of the rockslides head scarp). In addition, two different joint sets were observed; the first striking ESE and dipping with 10–25°

towards NNE, and the second with a NE strike and subvertical dip. Figure 9 illustrates a Google Earth® view and the geomodel with the implemented structural data.

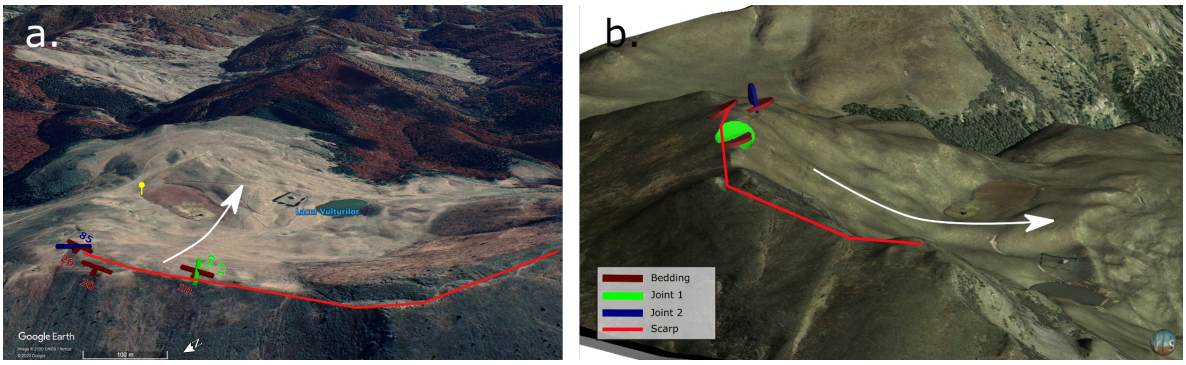

Figure 9. (**a**) Google Earth® views of the Eagle's Lake rockslide with the strike-dip symbols of the measurement. The yellow icon has as coordinates of latitude 45°30′43.90″ N and longitude 26°8′6.76″ E. (**b**) 3D geomodel of the Eagle's Lake rockslide with a view towards the NE, the disks mark the local strike and dip orientation.

3.4. Geomodel of the Balta Rockslide

The Balta rockslide is a typical anti-dip slope case (i.e., dip of bedding into the slope) as also mentioned by Micu et al. [60]. The field measurements implemented in Google Earth® images and stereographic projections (Figures 10 and A3) show three main structural features: bedding planes and two joint sets.

The results from the stereonet (Figure A3) reveal the anti-dip character of the bedding planes, the favourable azimuth of the dip in the direction of the slide for one family of joints and the plane of detachment for the second family of joints. Bedding planes are mainly dipping S-SE, with a N48° E 40° S Fisher mean plane. Figure 11 clearly highlights the anti-dip character of the bedding. The first family of joints (green), with the mean Fisher plane oriented N241° E 56° NW, shows patterns favouring instability, marked by an average trend in the direction of the sliding. Finally, the second family of joints (blue), has a Fisher mean plane oriented N133° E 74° SW and displays patterns favouring detachment.

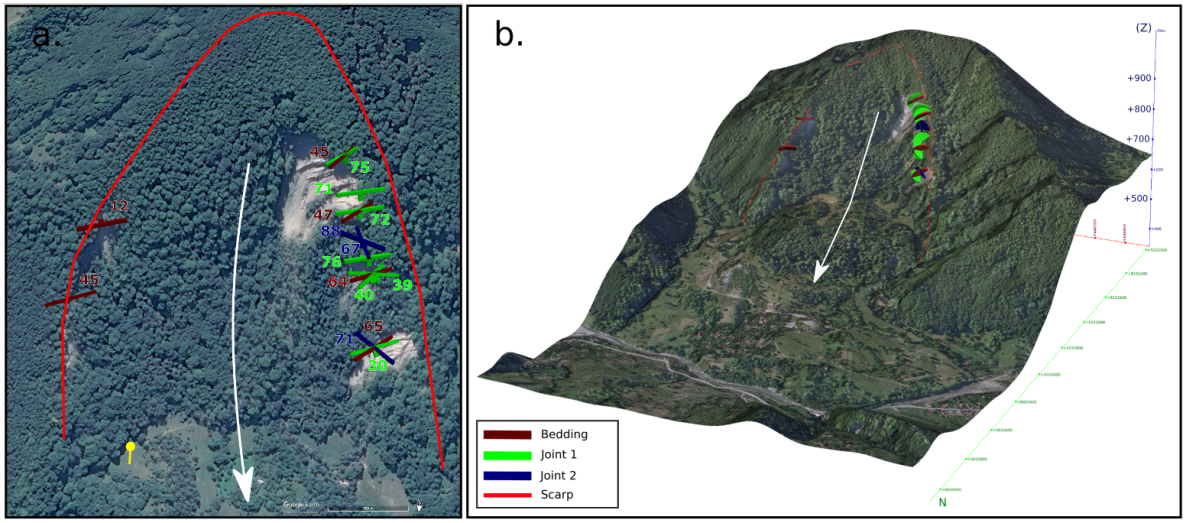

Figure 10. (**a**) Google Earth® views of the Balta rockslide with the strike-dip symbols of the measurement. The yellow icon has as coordinates of latitude 45°26′51.03″ N and longitude 26°21′2.64″ E. (**b**) 3D geomodel of the Balta rockslide with a 3D stereonet (view towards the south), the disks mark the local strike and dip orientation.

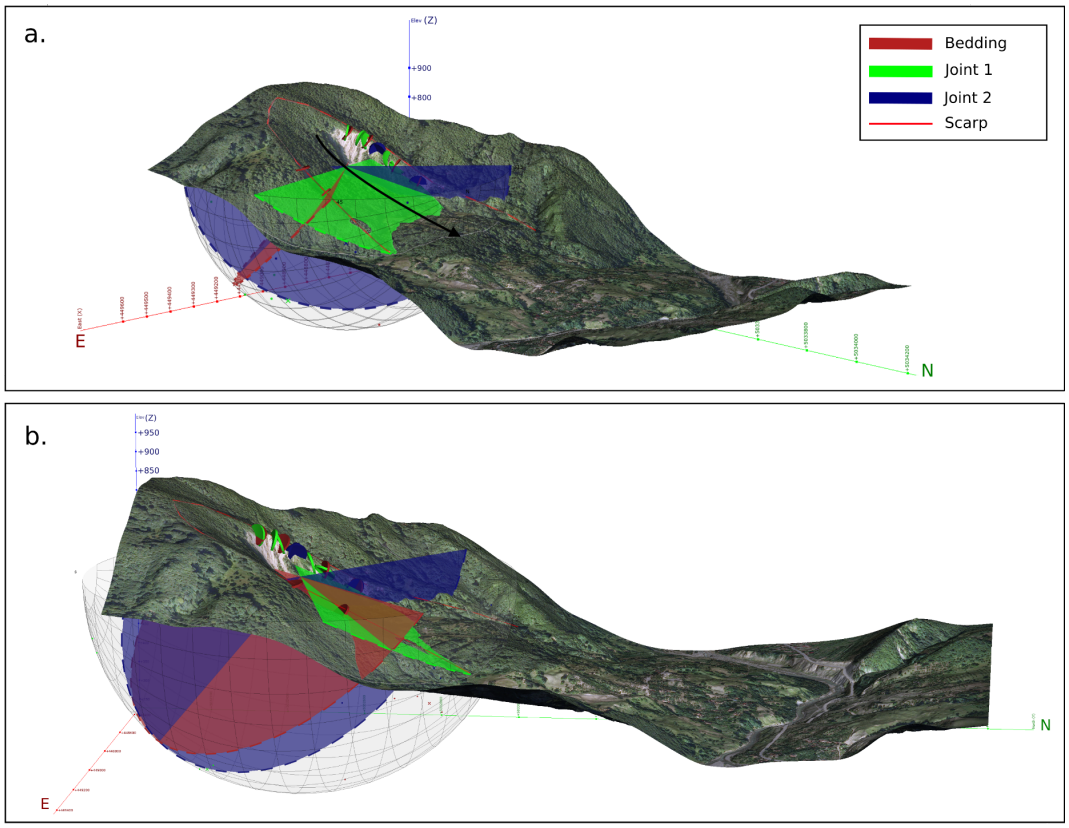

Figure 11. 3D geomodel of the Balta rockslide with a 3D stereonet; (**a**) view towards the SW and (**b**) view towards the W. The coloured planes are the Fisher mean planes and the disks mark the local strike and dip orientation (coordinate system: UTM 35N).

In the case of the Balta slide, the created geomodel is the basis for further numerical analyses, as presented in the following. It allows a better understanding of the geological and structural context of the site, and facilitates the reconstruction of a pre-failure morphology of the slope (based on volume estimations of the displaced mass).

4. Static and Dynamic 2D Numerical Models of the Balta Rockslide

For further investigations on the impact of slope morphologies, and especially, their internal structures, the Balta rockslide was determined as test site and analysed with the distinct element code UDEC by Itasca®. The 2-dimensional code, developed for discontinuous problems, allows one to quantify the effects of loads and external stresses applied to jointed rock material by combining two numeric approaches: the distinct element method (DEM) and the finite-difference method (FDM). On the basis of 2D sections of Balta, three slope morphologies were created, differing in terms of steepness—gentle, medium, and steep. In addition, eight structural models were defined varying in dip angles of internal bedding planes and joint sets. For these models, several scenarios were tested by applying static and dynamic loading, i.e., gravitational forces and seismic shaking, respectively. The results of the numerical analysis are presented in terms of displacement magnitudes, thereby quantifying the static behaviour of the slope, and the potential impact of seismic wave propagation through the slope. Similar studies have been presented by, e.g., Pal et al. [61] and Li et al. [62].

4.1. Modelled Slope Morphologies and Rock Structures

On the basis of the actual morphology of the Balta rockslide and analyses of the failed rock volume (presented in Mreyen et al. [63]), a possible slope surface prior to failure was created. The volume

balance of pre and post-failure state of the slope (considering a bulking factor of 15%, i.e., volume expansion during collapse; cf. Jaboyedoff et al. [64]) was established in its 3D geomodel. Here, a 2D section was extracted from the latter and used as input profile in UDEC. The chosen cross-section is located in the central part of the slope and is shown in Figure 12 with the actual and estimated pre-failure slope surfaces. This slope morphology is referred to as "medium slope" and represents the most realistic scenario. Although we analysed two additional morphologies ("gentle" and "steep"), only the medium slope morphology is considered to represent realistic pre-failure conditions. For the creation of the gentle and steep surfaces, the medium slope angle (∼40°) was decreased by ∼15° and increased by ∼65°, respectively (Figure 13). These altered surfaces are used for comparisons to outline the influence of slope gradient (in combination with various rock structures) on deformation patterns.

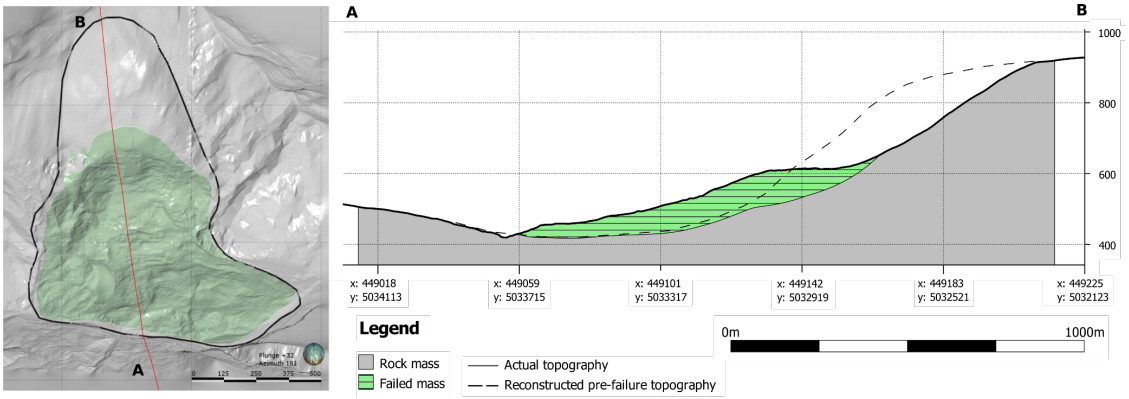

Figure 12. Cross section A–B of the Balta rockslide (location marked by the red line in the left figure with the estimated debris mass coloured in green) and its reconstructed pre-failure topography (dashed line).

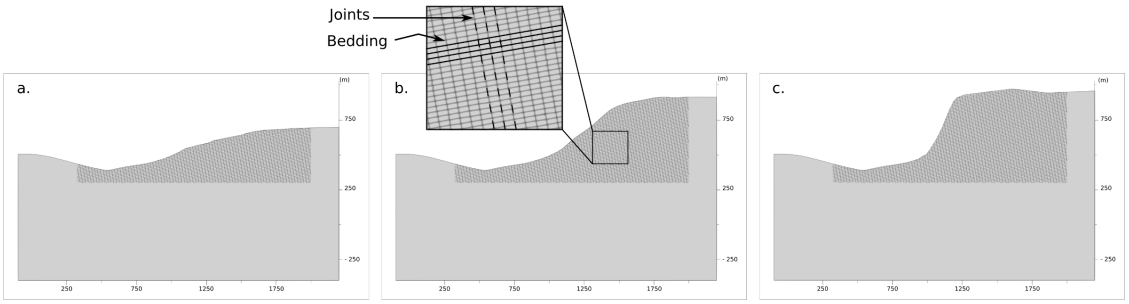

Figure 13. Three slope morphologies corresponding to (**a**) a gentle slope; (**b**) a medium slope (Balta case); (**c**) a steep slope.

In a next step, internal slope structures were defined: the orientations of the bedding planes and intersecting joint sets. The structures are used as inputs for a parametric study of the influence of varying bedding and joint orientations on static and dynamic deformation. In the UDEC simulations, these structures are modelled as discontinuities separating block elements; their assigned geomechanical properties are listed in Table 2. The elastic properties of the internal block material are listed in Table 3. For all models, a density ρ of 2400 kg/m^3, a bulk modulus K of 9.59 GPa, and a shear modulus G of 4.06 GPa were applied. These properties were estimated from geophysical studies performed in the study area; to represent non-fragmented rock material of a pre-failure state, the elastic properties were deduced from surveys of intact rock material, i.e., on bedrock or at depths unaffected by failure. Results of the geophysical surveys are documented in the parallel work of Mreyen et al. [63]. Note, for the discontinuities (Table 2), we used a parametric approach by assigning different geomechanical properties to the different slope models, i.e., shear resistance increasing with the steepness of the slope model in order to reproduce initial stability. The same approach was used for the varying c-φ values of the block material in Table 3.

Table 2. Geomechanical properties of the discontinuities: bedding planes (**b**) and rock joints (**j**); residual properties are marked by the suffix *r* (ks-joint shear stiffness; kn—joint normal stiffness; φ—friction angle; *c*—cohesion).

Slope	ks [GPa]	kn [GPa]	φ [degree]	*c* [MPa]	bφ_r [degree]	bc_r [MPa]	jφ_r [degree]	jc_r [MPa]
Gentle	0.5	1	30	0.1	20	0	25	0.05
Medium	0.5	1	35	0.2	25	0.1	30	0.15
Steep	0.5	1	45	1	35	0.3	40	0.5

Table 3. Elastic properties of the block material (ρ—density; *K*—bulk modulus; *G*-shear modulus; φ—internal friction angle; *c*—internal cohesion).

Slope	ρ [kg/m^3]	*K* [GPa]	*G* [GPa]	φ [degree]	*c* [MPa]
Gentle	2400	9.59	4.06	30	0.1
Medium	2400	9.59	4.06	35	0.2
Steep	2400	9.59	4.06	45	1

By varying the slope angle and discontinuity orientations, a total of fourteen static and corresponding dynamic model sections were obtained (Table 4). These different slope models were created to test the influences of structures on the slopes; these simulations were not really completed to back-analyse the specific case of the Balta rockslide, which corresponds the middle slope. A continuous spacing was defined for the modelled discontinuities: 20 m for the bedding; 40 m for the joints.

Table 4. Bedding and joint structures simulated in UDEC for each slope (b = bedding and j = joints).

Models	Gentle Slope	Medium Slope	Steep Slope
(**1**) b: 10° dip-j: 80° anti-dip	x	x	x
(**2**) b: 80° anti-dip-j: 10° dip	x	x	x
(**3**) b: 10° anti-dip-j: 80° dip		x	x
(**4**) b: 80° dip-j: 10° anti-dip		x	x
(**5**) b: 35° dip-j: 55° anti-dip		x	
(**6**) b: 55° anti-dip-j: 35° dip		x	
(**7**) b: 50° dip-j: 40° anti-dip		x	
(**8**) b: 40° anti-dip-j: 50° dip		x *	

* corresponds to the Balta case.

4.2. Static Analysis of the 2D Balta Models

To clarify the influences of the bedding and joint structures on the slope stability we first performed a static analysis. As mentioned before, three morphological slopes (gentle, medium, and steep) were studied and a total of fourteen models were created. The boundary conditions chosen for the static model domain fix the velocity and stress of deformable blocks at the lateral borders (velocity in x-direction) and at the model bottom (velocity in y-direction); viscous damping with a ratio of damping dissipation to kinetic energy change of 0.5 was applied to all blocks. The rock blocks were dry, water was incorporated into the models. Furthermore, only one material composed the slope; the constitutive model chosen for the deformable blocks was the Mohr–Coulomb plasticity model. A static loading was performed on each model until stabilisation in order to simulate the effect of gravity and the mechanical forces acting on the modelled rock blocks. Here, large displacement distributions will be analysed even though other small displacements may also indicate particular patterns, but these are difficult to interpret as they are due only to small deformation. The static models are presented in Figure 14 in tabular form separated in columns according the slope morphology and by rows according to the structure. Here, only large displacement distributions will be analysed, even though other small displacements may also indicate particular patterns, but these are difficult to interpret as they are due only to small deformation. From these

large distributions it can be concluded that the static models are relatively stable. The maximum displacement observed was 0.5 m for structure 2 (b = 80° anti-dip and j = 10° dip) with a steep slope. Structure 2 with an average slope also showed the largest displacement up to 0.4 m. Structure 5 with an average slope produced a displacement up to 0.3 m at the bottom of the slope. All the other structures did not show significant deformation.

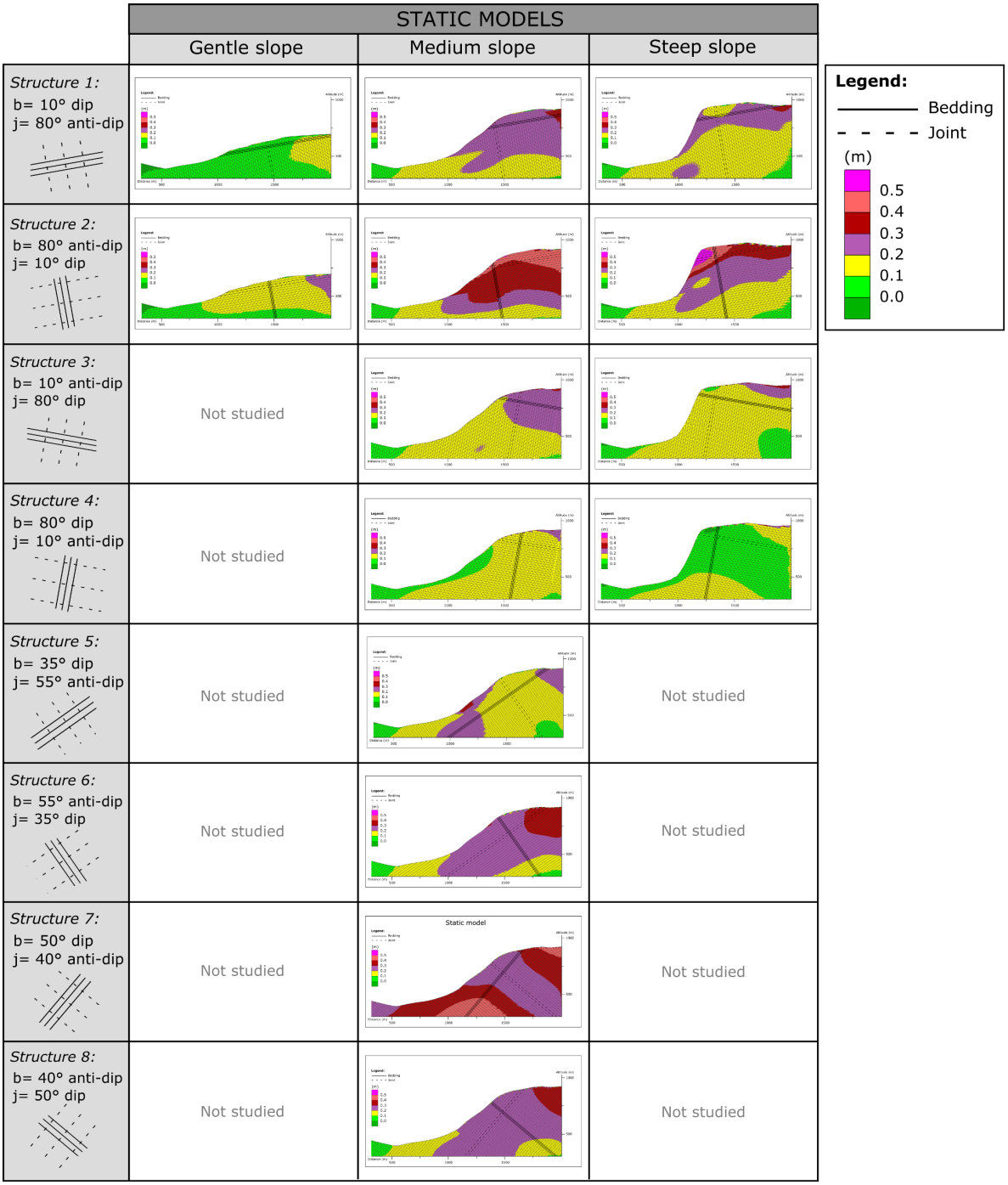

Figure 14. Static modelling results in terms of displacements for the three rock slope cases.

4.3. Dynamic Analysis of the 2D Balta Models

To further investigate the influences of the bedding and joint structures, we studied the responses of the models when subjected to a dynamic load, such as a seismic wave resulting from an earthquake. The dynamic loading was propagated from the bottom of each model during a cycle of 10 s in the

form of a synthetic Ricker wavelet (presenting two dominant frequency values 1.4 and 3.5 Hz). For the dynamic model domain, we chose free-field boundary conditions at the lateral model boundaries, while a viscous boundary was applied to the bottom of the model. We, furthermore, applied Rayleigh damping of 2% around the used central frequency of 2.5 Hz (for geological materials a Rayleigh damping of 2–5% is recommended; cf. [65]). The results of the dynamic models (Figure 15) show that permanent displacements are significantly larger than in the static models (along the slope-only considering those displacements related to sliding motion, not those due to general model adaptation during static gravitational loading—which might be bigger in the static case). For all the different slope inclinations, the largest displacements were again observed for structure 2 (b = 80° anti-dip and j = 10° dip). The steep slope (structure 2) was the most affected by dynamic wave propagation with a displacement magnitude up to 1.8 m; the deformation was located at the upper part of the slope. The model marked by a medium slope and structure 2 also presented large deformations along the whole slope and crest. This displacement pattern is in contrast with the one produced by structure 1, wherein a large deformation was rather restricted for all types of slope inclination and concentrated on the bottom of the slope for the gentle slope. Structure 5 (b = 35° anti-dip and j = 55° anti-dip) displayed near-surface displacements up to 0.8 m with a shape clearly influenced by the bedding. The displacements in structure 8 (b = 40° anti-dip and j = 50° dip), corresponding to the Balta rockslide, were characterised by a lenticular shape. The bottom and upper parts of the slope were influenced by these deformations (0.4 m). Structures 3-4-6-7 did not produce significant displacements, even after seismic shaking. Structure 6, however, showed minor deformations of 0.35 m following the joint inclination.

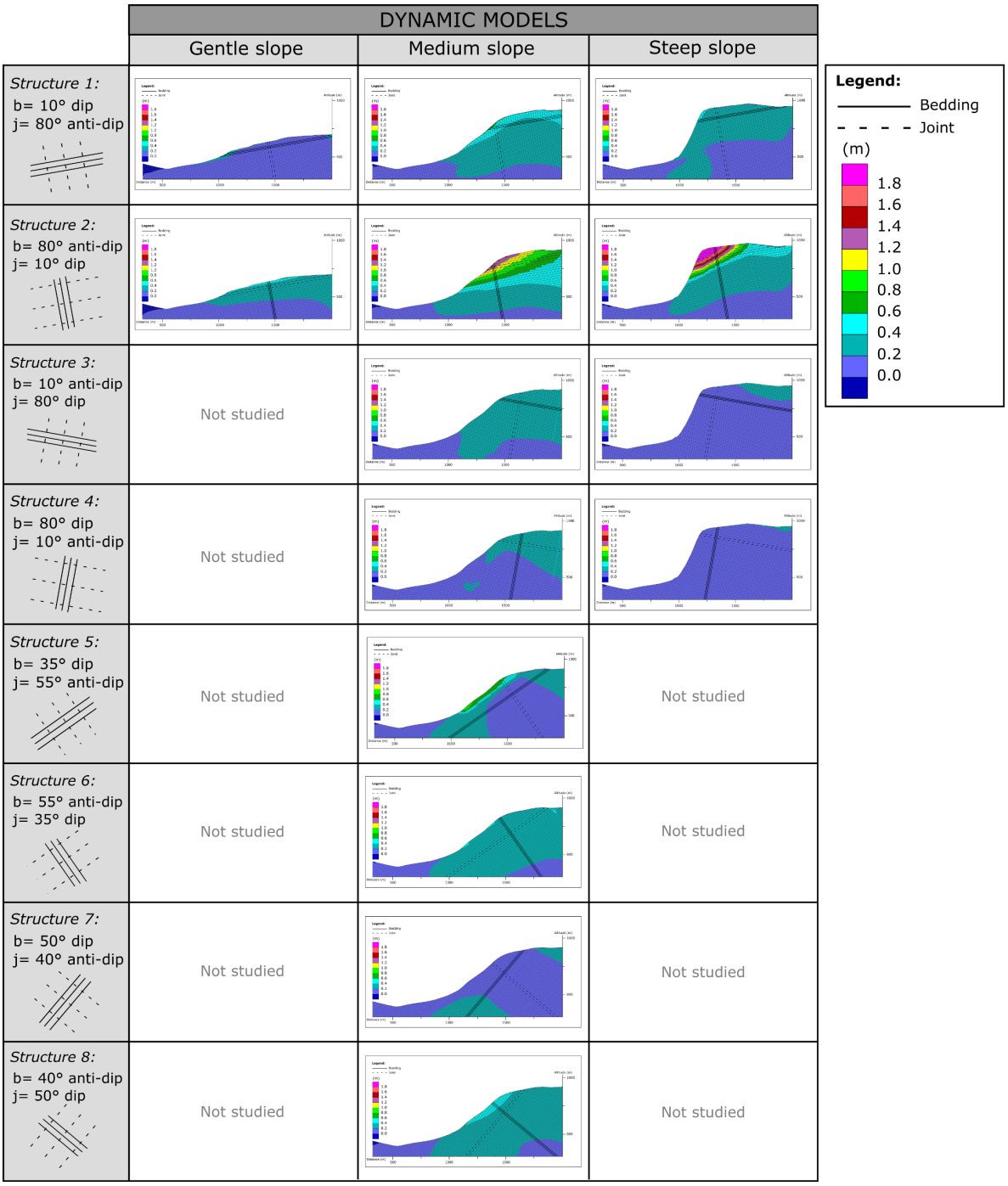

Figure 15. Dynamic modelling results in terms of displacements for the three rock slope cases.

5. Discussion

5.1. Influence of Slope Versus Orientation of Discontinuity on Slope Stability

First, we will focus on the displacement sections (Structures 6 and 8; Figure 16) produced by dynamic modelling for the two cases closest to the Balta morphology and structure, with a medium slope and 40° to 55° anti-dip slope bedding structure. The results indicate that minor displacements occurred after simulated shaking, whereas under static conditions the slope showed no deformations.

	Medium slope (Dynamic models)
Rock material	φ= 35°
	coh= 0.20 MPa
Joints	φ= 35° --> φres= 30°
	coh= 0.20 MPa --> cohres= 0.15 MPa
Bedding	φ= 35° --> φres= 25°
	coh= 0.20 MPa --> cohres= 0.10 MPa
Structure 6: b= 55° anti-dip j= 35° dip 	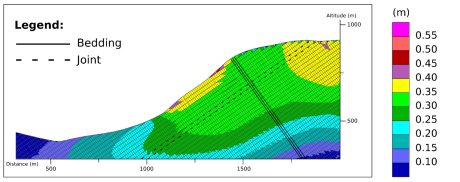 *Dynamic displacements (0-0.55 m)*
Structure 8: b= 40° anti-dip j= 50° dip 	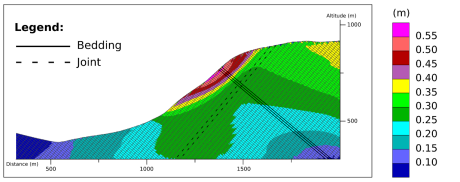 *Dynamic displacements (0-0.55 m)*

Figure 16. Dynamic modelling results (in terms of displacements) for the rock slope conditions closest to the Balta case, with anti-dip slope bedding structure.

In fact, only the steep-slope case with 80° anti-dip slope bedding structure (structure 2) produced significant displacements (0.3 m) after gravitational loading. Indeed, this same bedding structure was the one most affected by the dynamic input, as 0.5 m displacements could be simulated for all slope morphologies, even for the gentle one (Figure 17). Interestingly, the 80° dip slope bedding structure did not produce any significant (>0.3 m) displacement after shaking, for any slope morphology or structure. We attribute this to the toppling and detachment process affecting the 80 anti-dip slope structure (also under static conditions, strongly accentuated by shaking). This process potentially leads to the collapse of the whole upper part (above mid-slope position) of the steep and medium slope. For the latter the deformation could be very deep (more than 100 m deep), whereas only some 0.5 m deformation occurred near the surface over the convex curved part of the more gentle slope.

The dynamic results of structures 6 and 8 highlight that a small change in the inclination of the bedding can have a strong influence on the displacement.

	Dynamic models		
	Gentle slope	Medium slope	Steep slope
Rock material	φ= 30°	φ= 35°	φ= 45°
	coh= 0.10 MPa	coh= 0.20 MPa	coh= 1.0 MPa
Joints	φ= 30° --> φres= 25°	φ= 35° --> φres= 30°	φ= 45° --> φres= 40°
	coh= 0.10 MPa --> cohres= 0.05 MPa	coh= 0.20 MPa --> cohres= 0.15 MPa	coh= 1.0 MPa --> cohres= 0.50 MPa
Bedding	φ= 30° --> φres= 20°	φ= 35° --> φres= 25°	φ= 45° --> φres= 35°
	coh= 0.10 MPa --> cohres= 0.00 MPa	coh= 0.20 MPa --> cohres= 0.10 MPa	coh= 1.0 MPa --> cohres= 0.30 MPa
Structure 2: b= 80° anti-dip j= 10° dip 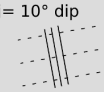	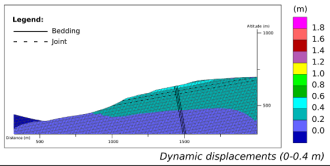 *Dynamic displacements (0-0.4 m)*	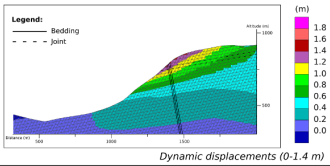 *Dynamic displacements (0-1.4 m)*	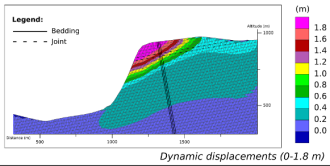 *Dynamic displacements (0-1.8 m)*
Structure 4: b= 80° dip j= 10° anti-dip 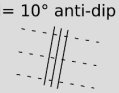	Not studied	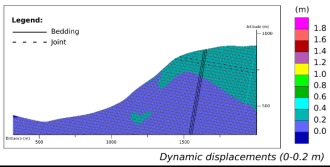 *Dynamic displacements (0-0.2 m)*	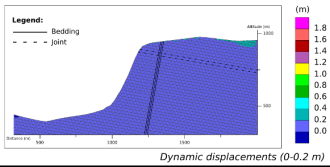 *Dynamic displacements (0-0.2 m)*

Figure 17. Dynamic modelling results (in terms of displacements) for the three rock slope cases with structure 1 and 2.

The results of numerical simulations (Figure 16) show that the displacement distribution induced by seismic shaking is not directly influenced by the rock structure. If the model allowed for it, larger deformation induced by larger shaking would cut through the structures (this is not possible with UDEC since the material within the blocks must stay intact), as it could be observed for most of these rockslide scarps—noting that some bedding failure could nevertheless be observed in the central part of, e.g., the Tamins rockslide scarp. We have not studied rockslides in the field that failed from very steep slopes—so the simulated effect of rock colon toppling on final failure cannot be directly compared with our observations; however, the existence of this deformation pattern and its influence on massive failure is relatively well known [62,66,67].

The cases of the Tamins and Fernpass rockslides could not be analysed in UDEC (in 2D) as the results for the Tamins rockslide would only be valid for the central part of the rockslide (with dip-slope structure) and not for the borders where bedding is oblique to sliding. Furthermore, for the Fernpass rock avalanche a three-dimensional numeric analysis would be required to fully comprehend the site.

5.2. Specific Deformation Patterns of Seismically-Induced Rock Slope Failure

The dynamic analysis highlights specific deformation patterns during seismic shaking, depending on the orientations or joints and bedding planes. The model with anti-dip slope bedding plane structure (medium slope) can potentially produce rotational sliding (Figure 16). Models with structure 1 (medium and steep slope) and structure 2 (medium and steep slope) produced toppling-detachment. The structure 2 with 80° anti-dip slope bedding produces much larger displacements (both in static and dynamic) than the 80° dip-slope bedding as shown in Figure 17. For the 80° anti-dip slope the rock columns can develop flexural toppling failure, get detached (as low cohesion on bedding planes, see in Section 4.1) and then slide along favourably oriented joints (even though only 10° dip). The 80° dip in the direction of the slope is too large to allow for sliding (bedding planes do not cross the slope surface) and the joints with 10° anti-dip slope are not favourably oriented. We attribute this surprising result that the 80° anti-dip slope bedding (with 10° joint dip slope-structure 2) orientation induces much larger displacements than the favourably oriented 10° dip slope bedding (with 80° joint anti-dip slope-structure 1) to the fact that, for the 80° anti-dip slope bedding (structure 2), the displacements are most likely caused by bending of relatively thin rock columns (20 m spacing between bedding planes). In the other case, with the 10° dip slope bedding (structure 1), the rock columns are thicker (40 m spacing between joints) and thus do not easily bend. Additionally, the 10° dip either of bedding or of joints along the slope is too small to allow for sliding (the friction angle is much larger). The flexural toppling can also explain why 0.5 m displacements were even reached for the gentle slope subjected to dynamic loading.

5.3. Tamins, Fernpass, Balta, and Eagle's Lake Rockslides—Seismically Triggered?

The different rockslides in the Alps (Tamins and Fernpass rockslides) and the Carpathians (Balta and Eagle's Lake rockslides) present similarities with rockslides that occurred in the Tien Shan (Ananevo, Bielogorka, Karasuu, and Belaldy rockslides) and which were most likely (or are known to have been) triggered by earthquakes. The common characteristics of all rockslides are the deep scarps, partially due to wedge failure and/or failure that "cuts" through geological structures (bedding and/or joint planes) across compact rocks. All scarps also formed at a high position of the slope; hence undercutting by river erosion can be excluded as a triggering factor. These can be identified as classical features for rockslides (or any landslides) of potential or certain seismic origin. However, the likelihood of a seismic origin also depends on the general seismic and climatic conditions. In this regard, prehistoric rockslides in the Tien Shan can be more easily classified as seismic, as seismicity is high and the climate is relatively arid (much drier than in the Alps, for example). Additionally, the Tien Shan was much less affected by glaciation than the Alps during the Pleistocene. Consequently, for very old rockslides located at an altitude of less than 3000 m a.s.l., glacial debuttressing can generally be excluded as a predispositional factor. This is different for the Alps—but similar for the Carpathians

(the studied region in the Carpathians has not been affected by extensive glaciation). In the Alps, glacial debuttressing and the higher amount of precipitation always have to be taken into consideration as factors influencing rock-slope stability. This is particularly true for rockslides that occurred soon after deglaciation, such as the Tamins rockslide—whereas glacial debuttressing probably influenced the triggering of the much younger Fernpass rock avalanche less. For that reason, it is interesting to consider rockslides in the Tien Shan (or other arid mountain regions—such as the Altai Mountains) as examples for seismically-triggered rockslides, as the origin of prehistoric cases is more likely connected with a seismic than with a climatic event.

The structural analysis of the studied rockslides reveals that for the Balta rockslide, the anti-dip slope structure is clearly unfavourable for sliding, but one joint set showed a favourable pattern for detachment. Furthermore, the numerical simulation of the case close to Balta (medium slope with the structure 8) showed that in static conditions the slope is stable, whereas when subject to shaking, it shows potential deformation. The Eagle's Lake rockslide is located in to the West of Balta, at a higher altitude, and is also partly marked by anti-dip slope failure. Here, the bedding has a lower dip as the rockslide is located close to a syncline axes in compact Cretaceous rocks. Additionally, the morphology of the site shows that the mountain top failed (the present altitude is certainly 50 m lower than before the mass movement occurred), which is a common feature of seismically induced rockslides. Additionally, this slope is located far from any river which excludes the possibility of slope failure by fluvial undercutting. However, the question still remains—did the same earthquake trigger both the Eagle's Lake and the Balta rockslides? Dating of those sites should provide an answer (planned for the next years).

Concerning the Tamins rockslide, the bedding orientation is changing but does not show a structure favouring failure everywhere; the most likely failure mode is the one of a wedge failure. There, the observations showed that rocks were intensively fractured and that only the combination of all joints would produce a common vector with a trend allowing for sliding. The rock mass of the Fernpass rock avalanche moved roughly along strike, which is not a clearly favourable structure for instabilities. Additionally, the scarps of the Fernpass and Tamins rockslides are laterally closed, which adds lateral friction and hampers the movement. Notwithstanding this lateral friction and unfavourable structure, the rocks were extruded from the Fernpass and Tamins mountains and became very mobile. However, it must be considered that the Tamins rockslide occurred at a time of climate changing to wetter and warmer conditions after the glaciers retreated [28], whereas Fernpass rock avalanche is much younger and was not influenced by immediate post-glacial changes in climate or slope debuttressing. It is therefore more likely that Fernpass has a seismic origin, whereas Tamins requires further analyses to conclusively constrain its age.

Very deep-seated scarps and their locations along the slope can be indicative of seismic triggering of massive slope failures with detachment scarps located close to the mountain ridge [5,10,68]. Those scarps are found in the Tien Shan, the European Alps, and the Carpathians; there are striking examples in the European Alps—the scarps of the Fernpass rock avalanche and of the Tamins rockslide, which thus hints at a (partial) seismic origin; and both rockslides (at least for the source zone part) look very similar, for instance, to the so-called Bielogorka "twin rock avalanches" in northern Tien Shan, which have a very likely seismic origin (that still has to be proven as well, as indicated by Havenith et al. [46]).

6. Conclusions

In this paper we presented structural geology information for several rockslides which display some characteristics of seismic triggering: they present a very deep scarp high on the slope, do not appear to have been influenced by river undercutting, and seem to have been formed in a statically stable condition. The motivation of this study was the expectation that certain rock structures can have a strong influence on slope stability and may be more or less susceptible to seismically induced failures. The Balta rockslide in Romania is the prime example of an ancient, massive slope failure

whose origin is unknown but for which a seismic origin is very likely since that site is composed of an initially stable bedding structure, dipping into the slope with 35° to 50°, locally including very thick (>5 m) sandstone beds. We arrived at a similar conclusion for the Eagle's Lake rockslide. For the Tamins rockslide source zone, a mixed situation can be observed, as rocks outcropping in the lateral parts of the scarp are overall not favouring massive slope failure (dip orientation very oblique to the sliding direction), whereas the central zone is marked by the presence of rock layers dipping in the same direction as the sliding movement (towards the south). Considering this central zone favouring instability and discontinuities aligning to facilitate wedge failure, a seismic influence cannot be easily proved for this mass movement. Additionally, the Tamins rockslide is likely to be the oldest one analysed here (even though we do not know the ages of the Romanian rockslides). The (most likely younger) Flims rockslide probably occurred at around the Proboreal/Boreal transition, when the valley was ice-free (cf. Ivy-Ochs et al. [28] and references therein), which would imply instability caused by climate changes, not requiring any seismic input. The much younger Fernpass rock avalanche, however, presents an unusual type of along-strike failure (similar to the Daguanbao rockslide triggered by the Wenchuan earthquake in 2008). The possible/partial seismic contribution to its development is much more likely than for the Tamins case and is thus worth being studied in more detail (including a more extensive structural analysis, geophysical surveys, studies of local hydrogeological conditions, geomechanical tests of rock samples, and a full dynamic back-analysis). This contribution could either have been the direct triggering of the massive failure or its preparation (as assumed by Korzhenkov et al. [53], for the Karasuu rockslide in Kyrgyzstan). Possibly, this rockslide might even help assess seismic hazards over longer terms in Western Austria. Even more generally, cases such as the Karasuu and Fernpass rockslides show that such rockslides with likely (partial) seismic origin help complete paleoseismic records—considering that in some cases the determined (reliable) age of the rockslide might be slightly younger than the causative earthquake event. All these examples and the complexity of the ancient landslide–paleo-earthquake relationship will also be discussed in the same volume by Strom and Havenith (in preparation).

Author Contributions: Conceptualisation, H.-B.H., A.-S.M., and E.L.; methodology, formal analysis and validation, A.-S.M. and E.L.; investigation, E.L.; writing—original draft preparation, E.L.; writing—review and editing, H.-B.H., A.D., and A.-S.M.; visualization, E.L.; supervision, H.-B.H., A.D., and A.-S.M. All authors have read and agreed to the published version of the manuscript.

Funding: This research received no external funding.

Acknowledgments: We thank Mihai Micu, from Romania, for the support in the structural geological mapping survey in May 2019 in the Romanian Carpathian Mountains.

Conflicts of Interest: The authors declare no conflict of interest.

Appendix A

Table A1. Table case studies seismic triggered rockslides.

RS Name	Location	Failure Date	Volume [$10^6 m^3$]	Rock Type	Structural Predisposition	Scarp Geometry/Failure Type	Visited and/or Google Earth	Seismic Trigger Category	Magnitude	References
Tamins	Switzerland	>8 ka BP	1500	sed.	joint sets outline wedge-failure geometry	'amphitheatre'/from top	V	very uncertain	none	Poschinger et al. [22]
Saymareh	Iran	>8 ka BP	>10,000	sed.	dip-slope on anticline limb (<15° slope)	wide and high scarp/from top	GE	likely	likely > 7.5	Howells [69]
Fernpass	Austria	4.2 ka BP	1000	sed.	along-strike failure	'amphitheatre'/from top	V & GE	possible	likely < 7	Prager et al. [16]
Oeschinen See	Switzerland	2.4 ka BP?	30	sed.	dip-slope failure	wide and high scarp/from mid-slope	GE	possible	likely < 7	Köpfli et al. [70]
Diexi	China	>1000 years (react. In 1933)	>1000	sed.	along-strike failure	multiple deep-seated wedges/from top	V & GE	seismic reactivation confirmed, initial seismic triggering very likely	likely > 7.5	Fan et al. [71]
Kokomeren	Kyrgyzstan	>1000 years	>1000	sed & metam. -magm.	anti-dip slope	wide and high scarp/ from top	V & GE	likely	likely > 7	Strom [72]
Balta	Romania	>1000 years	30	sed.	anti-dip slope	'amphitheatre'/starting from mountain crest end	V	unknown	likely > 7.5	Mreyen et al. [43]
Eagle's Lake	Romania	>1000 years	8	sed.	anti-dip slope	wide scarp, from top	V	unknown	likely > 7.5	Mreyen et al. [43]
Karasuu	Kyrgyzstan	>1000 years	150	sed.	anti-dip slope	multiple deep-seated scarps, from mountain crest end	GE	likely	likely > 7	Korzhenkov et al. [53]
Dobratsch Mtn (6 RS)	Italy	1348	30	sed.		wide and high scarp, from top	GE	confirmed	6.9	Lenhardt [18]
Tour d'Ai	Switzerland	1584	10?	sed.	subhorizontal bedding	deep-seatd scarp, from top	V & GE	confirmed	6.5	Fritsche et al. [19]

Table A1. *Cont.*

RS Name	Location	Failure Date	Volume Volume [$10^6 m^3$]	Rock Type	Structural Predisposition	Scarp Geometry/Failure Type	Visited and/or Google Earth	Seismic Trigger Category	Magnitude	References
Ananevo	Kyrgyzstan	1911	15	metam.-magma.	no favourably dipping from top	wide scarp, from mountain crest end	V	confirmed	7.8	Havenith et al. [46]
Rawilhorn	Switzerland	1946	12	sed.	subhorizontal bedding	wide and high scarp, from top	V & GE	confirmed	6.1	Moore et al. [73]
Khait	Tadjikistan	1949		metam.-magma.	no favourably dipping joints/foliation	wide and high scarp, from top	V	confirmed	7.4	Evans et al. [74] & Havenith et al. [47]
Lituya Bay	Alaska	1958	30	metam.-magma.	dip-slope/toppling failure (high angle dip of foliation)	wedge-like, from slope break	GE	confirmed	7.8	Fritz et al. [75]
Nevados Huascaran	Peru	1970 (1962)	>50	volcanic?	dip-slope failure (explaining also 1962 event)	deep-seatd wedge, from top	GE	confirmed	7.8	Cluff [76]
Belaldy	Kyrgyzstan	1992	40	metam.-magma.	favourably oriented foliation	wide and high scarp, from top	V & GE	confirmed	7.2	Havenith et al. [47]
Hattian Bala	Pakistan	2005	100	sed.	along plunging syncline axis	wide wedge failure, high scarp, from top	GE	confirmed	7.6	Basharat et al. [77]
Daguanbao	China	2008	>1000	metam.-magma.	along-strike failure	'amphitheatre'/from top	V & GE	confirmed	7.9	Cui et al. [13]
Wenjiagou	China	2008	>100	sed.	dip-slope failure	wide and high scarp, from top	V & GE	confirmed	7.9	Fan et al. [71]

Appendix B

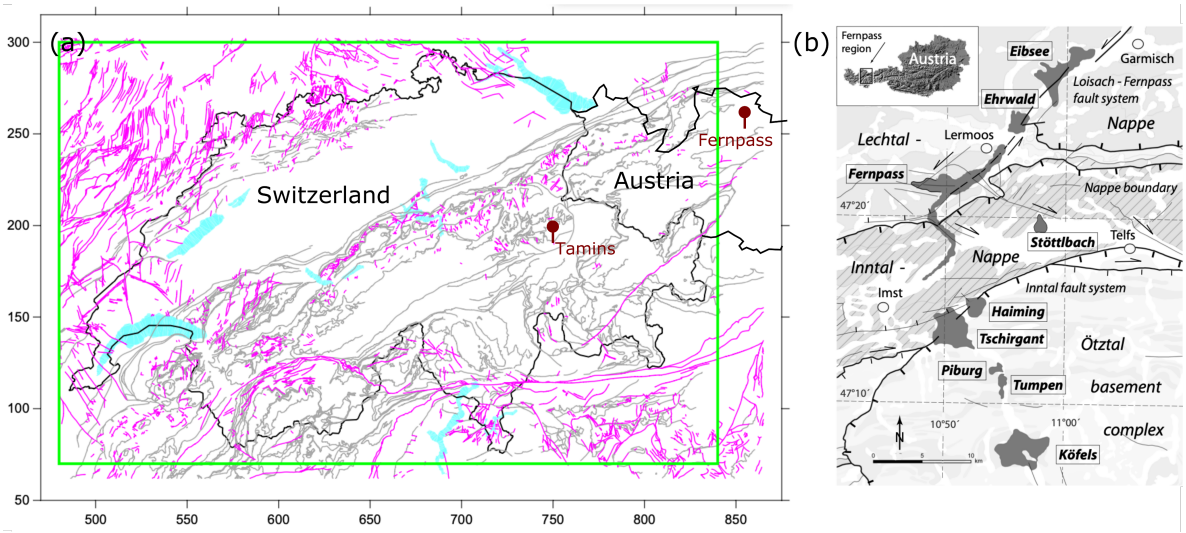

Figure A1. (**a**) Map view of the fault database held by the Swiss Federal Office of Topography, adapted from [29]. Supposedly-active and supposedly-inactive faults are, respectively, coloured in magenta and grey. (**b**) Main geological structures of the Fernpass region (Tyrol, Austria) highlighting thrust sheet units and deep-seated rockslide deposits (coloured in dark grey) and the left-lateral strike-slip fault system located in the east of the Fernpass source area (extracted from [16].)

Appendix C

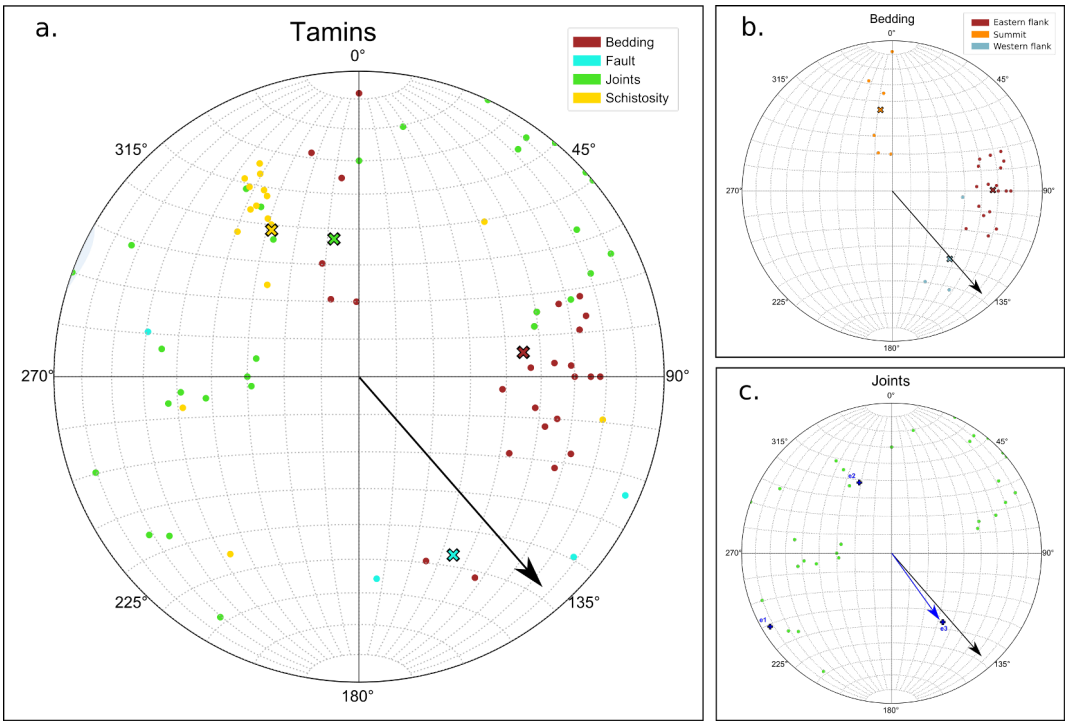

Figure A2. Stereonets of (**a**) all the structural data of the Tamins rockslide (**b**) data of the bedding and (**c**) data of the joints. Dots are the poles of the great circles and crosses are mean the poles. The blue crosses (e1, e2 and e3) are the three-axis of the Bingham best-fit plane. The blue arrow pointing e3, the trend and plunge, and the black arrow shows the direction of the slide.

Appendix D

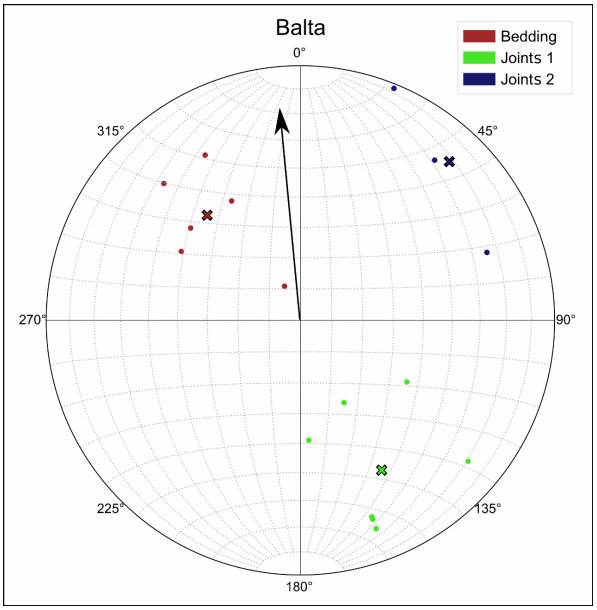

Figure A3. Stereonet of the structural data of the Balta rockslide. Dots are the poles of the great circles and crosses are mean the poles and the black arrow shows the direction of the slide.

Appendix E

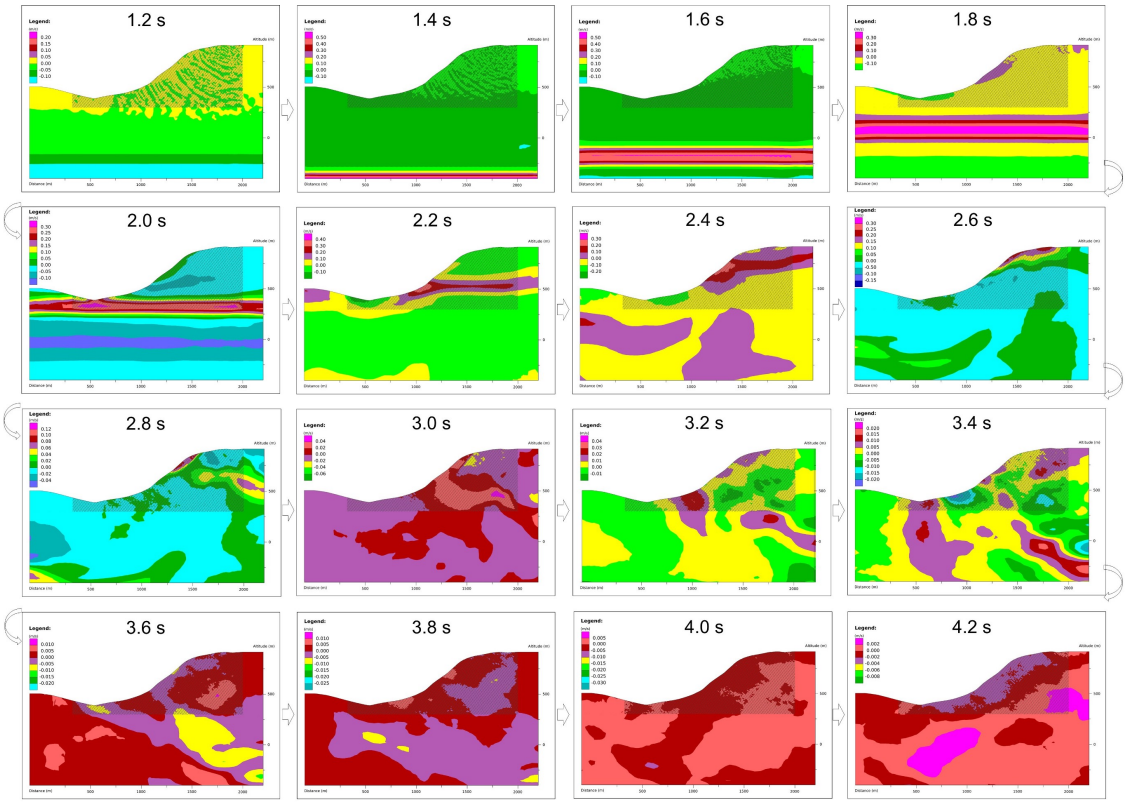

Figure A4. Dynamic modelling results for the rock slope conditions closest to the Balta case, with structure 8, plot with the xvelocity propagation (cyle time 0.2).

References

1. Heim, A. *Bergsturz und Menschenleben*; Beiblatt zur Vierteljahrsschrift der Naturforschenden Gesellschaft in Zürich; Fretz & Wasmuth: Zürich, Switzerland, 1932.
2. Abele, G. Bergstürze in den Alpen: Ihre Verbreitung, Morphologie und Folgeerscheinungen. In *Wissenschaftliche Alpenvereinshefte*; Dt. Alpenverein, Ed. 1974. Available online: https://pascal-francis.inist.fr/vibad/index.php?action=getRecordDetail&idt=PASCALGEODEBRGM7920324796 (accessed on 18 August 2020).
3. Korup, O. Geomorphometric characteristics of New Zealand landslide dams. *Eng. Geol.* **2004**, *73*, 13–35. [CrossRef]
4. Hewitt, K. Rock avalanches that travel onto glaciers and related developments, Karakoram Himalaya, Inner Asia. *Geomorphology* **2009**, *103*, 66–79. [CrossRef]
5. Strom, A.; Abdrakhmatov, K. *Rockslides and Rock Avalanches of Central Asia: Distribution, Morphology, and Internal Structure*; Candice Janco: Amsterdam, The Netherlands, 2018.
6. Jaboyedoff, M.; Carrea, D.; Derron, M.H.; Oppikofer, T.; Penna, I.M.; Rudaz, B. A review of methods used to estimate initial landslide failure surface depths and volumes. *Eng. Geol.* **2020**, *267*, 105478. [CrossRef]
7. Varnes, D.J. Slope movement types and processes. *Spec. Rep.* **1978**, *176*, 11–33.
8. Cruden, D.M. A simple definition of a landslide. *Bull. Int. Assoc. Eng. Geol.-Bull. De L'Association Int. De Géologie De L'Ingénieur* **1991**, *43*, 27–29. [CrossRef]
9. Cruden, D.M.; Varnes, D.J. Landslides: Investigation and mitigation. Chapter 3-Landslide types and processes. In *Transportation Research Board Special Report*; Transportation Research Board: Washington, DC, USA, 1996.
10. Davies, T.; McSaveney, M. Rock-Avalanche Size and Runout–Implications for Landslide Dams. In *Natural and Artificial Rockslide Dams*; Springer: Berlin/Heidelberg, Germany, 2010; pp. 441–462. [CrossRef]
11. Korup, O.; Clague, J.J.; Hermanns, R.L.; Hewitt, K.; Strom, A.L.; Weidinger, J.T. Giant landslides, topography, and erosion. *Earth Planet. Sci. Lett.* **2007**, *261*, 578–589. [CrossRef]
12. Keefer, D.K. Landslides caused by earthquakes. *GSA Bull.* **1984**, *95*, 406–421. [CrossRef]
13. Cui, S.; Pei, X.; Huang, R. Effects of geological and tectonic characteristics on the earthquake-triggered Daguangbao landslide, China. *Landslides* **2018**, *15*, 649–667. [CrossRef]
14. Keefer, D.K. Statistical analysis of an earthquake-induced landslide distribution — the 1989 Loma Prieta, California event. *Eng. Geol.* **2000**, *58*, 231–249. [CrossRef]
15. Parise, M.; Jibson, R.W. A seismic landslide susceptibility rating of geologic units based on analysis of characteristics of landslides triggered by the 17 January, 1994 Northridge, California earthquake. *Eng. Geol.* **2000**, *58*, 251–270. [CrossRef]
16. Prager, C.; Zangerl, C.; Patzelt, G.; Brandner, R. Age distribution of fossil landslides in the Tyrol (Austria) and its surrounding areas. *Nat. Hazards Earth Syst. Sci.* **2008**, *8*, 377–407. [CrossRef]
17. Wiemer, S.; Danciu, L.; Edwards, B.; Marti, M.; Fäh, D.; Hiemer, S.; Wössner, J.; Cauzzi, C.; Kästli, P.; Kremer, K. *Seismic Hazard Model 2015 for Switzerland (SUIhaz2015)*; Technical Report; ETH: Zurich, Switzerland, 2016. [CrossRef]
18. Lenhardt, W. Earthquake-triggered landslides in Austria–Dobratsch revisited. *Jahrb. Geol. Bundesanst.* **2007**, *147*, 193–199.
19. Fritsche, S.; Fäh, D.; Schwarz-Zanetti, G. Historical intensity VIII earthquakes along the Rhone valley (Valais, Switzerland): Primary and secondary effects. *Swiss J. Geosci.* **2012**, *105*, 1–18. [CrossRef]
20. Badoux, A.; Andres, N.; Techel, F.; Hegg, C. Natural hazard fatalities in Switzerland from 1946 to 2015. *Nat. Hazards Earth Syst. Sci.* **2016**, *16*, 2747–2768. [CrossRef]
21. Lateltin, O.; Haemmig, C.; Raetzo, H.; Bonnard, C. Landslide risk management in Switzerland. *Landslides* **2005**, *2*, 313–320. [CrossRef]
22. Poschinger, A.V.; Wassmer, P.; Maisch, M. the Flims Rockslide: History of interpretation and new insights. In *Landslides from Massive Rock Slope Failure*; Evans, S.G., Mugnozza, G.S., Strom, A., Hermanns, R.L., Eds.; Springer: Dordrecht, The Netherlands, 2006; pp. 329–356.
23. Poschinger, A.V. The Flims Rockslide Dam. In *Natural and Artificial Rockslide Dams*; Evans, S.G., Hermanns, R.L., Strom, A., Scarascia-Mugnozza, G., Eds.; Springer: Berlin/Heidelberg, Germany, 2011; pp. 407–421. [CrossRef]

24. Pollet, N.; Cojean, R.; Couture, R.; Schneider, J.L.; Strom, A.L.; Voirin, C.; Wassmer, P. A slab-on-slab model for the Flims rockslide (Swiss Alps). *Can. Geotech. J.* **2005**, *42*, 587–600. [CrossRef]
25. Krietsch, H.; Wolter, A. Preliminary forensic investigation of the structural and geomorphological controls on the prehistoric Tamins rockslide in Grisons, Switzerland. In *Landslides and Engineered Slopes. Experience, Theory and Practice*; CRC Press: Boca Raton, FL, USA, 2016; pp. 1205–1210. [CrossRef]
26. Poschinger, A.V.; Haas, U. Der Flimser Bergsturz, doch ein warmzeitliches Ereignis? *Bull. Angew. Geol.* **1997**, *2*, 35-46.
27. Deplazes, G.; Anselmetti, F.S.; Hajdas, I. Lake sediments deposited on the Flims rockslide mass: The key to date the largest mass movement of the Alps. *Terra Nova* **2007**, *19*, 252–258. [CrossRef]
28. Ivy-Ochs, S.; Poschinger, A.; Synal, H.A.; Maisch, M. Surface exposure dating of the Flims landslide, Graubünden, Switzerland. *Geomorphology* **2009**, *103*, 104–112. [CrossRef]
29. Hetényi, G.; Epard, J.L.; Colavitti, L.; Hirzel, A.H.; Kiss, D.; Petri, B.; Scarponi, M.; Schmalholz, S.M.; Subedi, S. Spatial relation of surface faults and crustal seismicity: A first comparison in the region of Switzerland. *Acta Geodaetica Geophysica* **2018**, *53*, 439–461. [CrossRef]
30. Ostermann, M.; Prager, C. Field Trip 12-Large-scale catastrophic rock slope failures in the Ötz-Inn-Loisach Valley region. *Geo. Alp* **2016**, *13*, 2257–2276.
31. Prager, C. Geologie, Alter und Struktur des Fernpass Bergsturzes und tiefgründige Massenbewegungen in seiner Umgebung (Tirol, Österreich). Ph.D. Thesis, University of Innsbruck, Innsbruck, Austria, 2010.
32. Mârza, V.; Pantea, A. Romania. History of earthquake hazards assessment. In *Stop Disaster, the Newsletter of the International Decade for Natural Disaster Reduction*; International Decade for Natural Disaster Reduction: Naples, Italy, 1991.
33. Bălteanu, D.; Chendeş, V.; Sima, M.; Enciu, P. A country-wide spatial assessment of landslide susceptibility in Romania. *Geomorphology* **2010**, *124*, 102–112. [CrossRef]
34. Micu, M. Landslide Types and Spatial Pattern in the Subcarpathian Area. In *Landform Dynamics and Evolution in Romania*; Springer: Berlin/Heidelberg, Germany, 2017; pp. 305–325.
35. Georgescu, E. the partial collapse of Coltzea Tower during the Vrancea earthquake of 14/26 october 1802: The historical warning of long-period ground motions site effects in Bucharest. In Proceedings of the International Conference Earthquake Loss Estimation and Risk Reduction, Bucarest, Romania, 24–26 October 2002.
36. Vacareanu, R.; Ionescu, C. *The 1940 Vrancea Earthquake. Issues, Insights and Lessons Learnt: Proceedings of the Symposium Commemorating 75 Years from November 10, 1940 Vrancea Earthquake*; Springer: Berlin/Heidelberg, Germany, 2016.
37. Rogozea, M.; Marmureanu, G.; Radulian, M.; Toma, D. Reevaluation of the macroseismic effects of the 23 January 1838 Vrancea earthquake. *Rom. Rep. Phys.* **2014**, *66*, 520–538.
38. Mândrescu, N. The Romanian earthquake of March 4, 1977; aspects of soil behaviour. *Revue Roumaine Géologie Géophysique Géographie Géophysique* **1981**, *25*, 35–56.
39. Radulescu, N.A. Considérations géographiques sur le tremblement de terre du 10 November 1940. *Comptes Rendus Séances LAcadémie Des Sciences Roumanie* **1941**, *5*, 243–269.
40. Radu, C.; Spânoche, E. On geological phenomena associated with the 10 November 1940 earthquake. *Revenue Romanian Geology Geophysics Geographic.–Geophysique* **1977**, *21*, 159–165.
41. Georgescu, E.S.; Pomonis, A. Building damage vs. territorial casualty patterns during the Vrancea (Romania) earthquakes of 1940 and 1977. In Proceedings of the 15th World Conference on Earthquake Engineering, Lisbon, Portugal, 24–28 September 2012; pp. 24–28.
42. Harta geologica 1:200000, f.C. *Geologic Map 1:200000, Covasna Sheet*; Geological Institute of Romania: Bucharest, Romania, 1968.
43. Mreyen, A.S.; Micu, M.; Onaca, A.; Cerfontaine, P.; Havenith, H.B. Integrated Geological-Geophysical Models of Unstable Slopes in Seismic Areas. In *Advancing Culture of Living with Landslides*; Springer International Publishing: Berlin/Heidelberg, Germany, 2017; pp. 269–279. [CrossRef]
44. Naum, T. *Observaţiuni Geomorfologice în Masivul Siriu*; Number 13; Analele University C.I. Parhon: Bucarest, Romania, 1957.
45. Sîrcu, I. Câteva precizări în legătură cu glaciaţia cuaternară din Carpaţii Orientali Româneşti. *Nat. Ser. Geol.-Geogr.* **1964**, *3*, 24–31.

46. Havenith, H.B.; Strom, A.; Jongmans, D.; Abdrakhmatov, A.; Delvaux, D.; Tréfois, P. Seismic triggering of landslides, Part A: Field evidence from the Northern Tien Shan. *Nat. Hazards Earth Syst. Sci.* **2003**, *3*, 135–149. [CrossRef]
47. Havenith, H.B.; Bourdeau, C. Earthquake-induced landslide hazards in mountain regions: A review of case histories from central asia (An inaugural lecture to the society). *Geol. Belg.* **2010**, *13*, 137–152.
48. Ignatiev, I. Earthquake in the Tokmak district in 1885. In *Proc. Imp. Russ. Geogr. Soc.* **1886**, *22*, 150–164.
49. Havenith, H.B.; Jongmans, D.; Faccioli, E.; Abdrakhmatov, K.; Bard, P.Y. Site Effect Analysis around the Seismically Induced Ananevo Rockslide, Kyrgyzstan. *Bull. Seismol. Soc. Am.* **2002**, *92*, 3190–3209. [CrossRef]
50. Havenith, H.B.; Strom, A.; Calvetti, F.; Jongmans, D. Seismic triggering of landslides. Part B: Simulation of dynamic failure processes. *Nat. Hazards Earth Syst. Sci.* **2003**, *3*, 663–682. [CrossRef]
51. Ghose, S.; Mellors, R.J.; Korjenkov, A.M.; Hamburger, M.W.; Pavlis, T.L.; Pavlis, G.L.; Omuraliev, M.; Mamyrov, E.; Muraliev, A.R. the MS = 7.3 1992 Suusamyr, Kyrgyzstan, earthquake in the tien shan: 2. Aftershock focal mechanisms and surface deformation. *Bull. Seismol. Soc. Am.* **1997**, *87*, 23–38.
52. Korjenkov, A.; Rust, D.; Tibaldi, A.; Abdiev, S. Parameters of the Strong Paleoearthquakes Along the Talas-Fergana Fault, the Kyrgyz Tien Shan. In *Earthquake Research and Analysis - Seismology, Seismotectonic and Earthquake Geology*; D'Amico, S., Ed.; InTech: London, UK, 2012. [CrossRef]
53. Korzhenkov, A.; Abdieva, S.; Belousov, T.; Rust, D.; Tibaldi, A. An age of rockslides and paleoearthquakes in the Karasu River valley (Talas-Fergana Fault, Kyrgyzstan). *Seism. Instrum.* **2014**, *50*, 97–108. [CrossRef]
54. Belousov, T.; Skobelev, S.; Strom, A. On estimation of the recurrence period of strong earthquakes of the central Tien Shan (according to data of absolute geochronology). *J. Earthq. Predict. Res.* **1994**, *3*, 226–236.
55. Havenith, H.; Strom, A.; Torgoev, I.; Torgoev, A.; Lamair, L.; Ischuk, A.; Abdrakhmatov, K. Tien Shan Geohazards Database: Earthquakes and landslides. *Geomorphology* **2015**, *249*, 16–31. [CrossRef]
56. Davis, G.H.; Reynolds, S. *Structural Geology of Rocks and Regions*, 2nd Ed.; JohnWiley & Sons: Hoboken, NJ, USA, 1996; p. 776.
57. Aber, J.; Ber, A. Glaciotectonism. In *Developments in Quaternary Sciences*; van der Meer, J.J., Ed.; Elsevier: Amsterdam, The Netherlands, 2007; Chapter 2, Volume 6, pp. 17–32. [CrossRef]
58. Love, J.J. Fisher Statistics. In *Encyclopedia of Geomagnetism and Paleomagnetism*; Springer: Dordrecht, The Netherlands, 2007; pp. 272–273. [CrossRef]
59. Allmendinger, R.W. *Stereonet Mobile for iOS v. 3.0*. 2017. Available online: http://www.geo.cornell.edu/geology/faculty/RWA/programs/stereonet-mobile-manual.pdf (accessed on 18 August 2020).
60. Micu, M.; Havenith, H.B.; Bălteanu, D.; Onaca, A.; Mreyen, A.S.; Cioflan, C. Certain and potential earthquake-induced landslides in Vrancea seismic region. In Proceedings of the 33rd Romanian Geomorphology Symposium, Iași, Romania, 11–14 May 2017. [CrossRef]
61. Pal, S.; Kaynia, A.M.; Bhasin, R.K.; Paul, D. Earthquake stability analysis of rock slopes: A case study. *Rock Mech. Rock Eng.* **2012**, *45*, 205–215. [CrossRef]
62. Li, L.Q.; Ju, N.P.; Zhang, S.; Deng, X.X.; Sheng, D. Seismic wave propagation characteristic and its effects on the failure of steep jointed anti-dip rock slope. *Landslides* **2019**, *16*, 105–123. [CrossRef]
63. Mreyen, A.S.; Cauchie, L.; Micu, M.; Onaca, A.; Havenith, H.B. Multiple geophysical investigation to characterize massive slope failure deposits: Application to the Balta rockslide, Carpathians. *Geophys. J. Int.* submitted.
64. Jaboyedoff, M.; Chigira, M.; Arai, N.; Derron, M.H.; Rudaz, B.; Tsou, C.Y. Testing a failure surface prediction and deposit reconstruction method for a landslide cluster that occurred during Typhoon Talas (Japan). *Earth Surf. Dyn.* **2019**, *7*, 439–458. [CrossRef]
65. Biggs, J. *Introduction to Structural Dynamics*; McGraw-Hill College: New York, NY, USA, 1964.
66. Glastonbury, J.; Fell, R. Geotechnical characteristics of large rapid rock slides. *Can. Geotech. J.* **2010**, *47*, 116–132. [CrossRef]
67. Majdi, A.; Amini, M. Flexural Toppling Failure in Rock Slopes: From Theory to Applications. *Int. J. Min.-Geo* **2011**, *45*, 21–32
68. Meunier, P.; Hovius, N.; Haines, J.A. Topographic site effects and the location of earthquake induced landslides. *Earth Planet. Sci. Lett.* **2008**, *275*, 221–232. [CrossRef]
69. Howells, D.A. A history of Persian earthquakes, by N. N. Ambraseys and C. P. Melville, Cambridge University Press, Cambridge, 1982. No. of pages: 219. Price: £35. *Earthq. Eng. Struct. Dyn.* **1983**, *11*, 591–591. [CrossRef]

70. Köpfli, P.; Grämiger, L.M.; Moore, J.R.; Vockenhuber, C.; Ivy-Ochs, S. the Oeschinensee rock avalanche, Bernese Alps, Switzerland: A co-seismic failure 2300 years ago? *Swiss J. Geosci.* **2018**, *111*, 205–219. [CrossRef]
71. Fan, X.; Yunus, A.P.; Jansen, J.D.; Dai, L.; Strom, A.; Xu, Q. Comment on 'Gigantic rockslides induced by fluvial incision in the Diexi area along the eastern margin of the Tibetan Plateau. *Geomorphology* **2019**, 338, 27–42. [CrossRef]
72. Strom, A. Mechanism of stratification and abnormal crushing of rockslide deposits. In Proceedings of the 7th International Association for Engineering Geology Congress, Lisboa, Portugal, 5–9 September 1994; Balkema: Rotterdam, The Netherlands, 1994.
73. Moore, J.; Gischig, V.; Amann, F.; Burjanek, J. Earthquake-triggered rock slope failures: Damage and site effects. In Proceedings of the 11th International & 2nd North American Symposium on Landslides, Banff, AB, Canada, 2–8 June 2012.
74. Evans, S.; Roberts, N.; Ischuk, A.; Delaney, K.; Morozova, G.; Tutubalina, O. Landslides triggered by the 1949 Khait earthquake, Tajikistan, and associated loss of life. *Eng. Geol.* **2009**, *109*, 195–212. [CrossRef]
75. Fritz, H.; Hager, W.; Minor, H.E. Lituya Bay case: Rockslide impact and wave run-up. *Sci. Tsunami Hazards* **2001**, *19*, 3–19.
76. Cluff, L.S. Peru earthquake of May 31, 1970; engineering geology observations. *Bull. Seismol. Soc. Am.* **1971**, *61*, 511–533.
77. Basharat, M.; Rohn, J.; Ehret, D.; Baig, M.S. Lithological and structural control of Hattian Bala rock avalanche triggered by the Kashmir earthquake 2005, sub-Himalayas, northern Pakistan. *J. Earth Sci.* **2012**, *23*, 213–224. [CrossRef]